Doctoral Dissertation

Analysis and Experiments of Parallel Line Feeders as a Practical Inductive Power Transfer System.

William-Fabrice BROU
Program of Information Science and Engineering
Graduate School of Science and Technology
Nara Institute of Science and Technology

Supervisor: Professor Minoru Okada
Network Systems Lab. (Division of Information Science)

Submitted on January 6, 2023

A Doctoral Dissertation
submitted to Graduate School of Science and Technology,
Nara Institute of Science and Technology
in partial fulfillment of the requirements for the degree of
Doctor of Engineering

William-Fabrice BROU

Thesis Committee:

Supervisor Minoru Okada
(Professor, Division of Information Science)
Yu-ichi Hayashi
(Professor, Division of Information Science)
Takeshi Higashino
(Associate Professor, Division of Information Science)
Duong Quang Thang
(Assistant Professor, Division of Information Science)

Analysis and Experiments of Parallel Line Feeders as a Practical Inductive Power Transfer System.[1]

William-Fabrice BROU

Abstract

Parallel line feeder (PLF) consisting of a two-wire transmission line operating in the MHz band has been proposed as a proof-of-concept with the promise of drastically reducing the cost and maintenance of inductive power transfer system while further increasing its range thanks to its simple and long structure. However, when it is long enough compared to the input signal wavelength, the PLF has the characteristic of transmission lines and suffers from the standing wave effect. This is an issue for the inductive power transfer as the PLF could not stably charge a receiver because the electromagnetic strength varies dynamically all over its length. In order to mitigate that standing wave effect, we first adopted a multiple-input multiple-output configuration of the PLF which consists of a series of parallel line feeders side-by-side and shifted in the longitudinal direction to expose and combine their different magnetic fields in a uniform way for better stability and higher output power. However, the use of multiple parallel lines feeders adds up to the cost and complexity of the system. More importantly, the efficiency of that first configuration is quite low due to the dielectric loss caused by the exposure of electric field to the surrounding materials. Therefore as improvement, a modified version of the system, where the PLF is divided into shorter segments which are concatenated and compensated by capacitors in order to mitigate the impact of the standing wave effect have been investigated through simulations and experiments. Their results show that the segmentation could display a near-uniform magnetic field strength capable of charging receivers

[1]Doctoral Dissertation, Graduate School of Science and Technology, Nara Institute of Science and Technology, January 6, 2023.

uniformly regardless of their positions on top of the line. In order for these investigations to be complete enough to show its performance as a practical system, the PLF has also been modeled as a lossy transmission line. In that configuration, the maximum achievable efficiency derived from the extended k-Q product formulation has been used as the upper-bound for the RF-to-RF efficiency of the PLF. The theoretical analysis shows that when the segments' lengths are properly determined, the segmentation scheme is able to improve and stabilize the efficiency all over the PLF length. Experimental results at 27.12 MHz with two different segmentation schemes confirm the theoretical analysis and show that a fairly high efficiency of 70% can be achieved when the segments are sufficiently short compared to the wavelength of the input signal frequency.

Keywords:

Parallel line feeder, standing wave problem, segmentation, capacitors compensation, efficiency stabilization, efficiency improvement.

Contents

List of Figures

List of Tables

1 Introduction

The first part of this chapter discusses the research motivation of the innovative parallel line feeder system. And then, the statement of the problem of the dissertation is presented. Next, the research contribution and scope will be discussed. The dissertation layout is shown at the end of this chapter.

1.1 Research motivation

Wireless Power Transfer starts became a universally adopted feature in the world of consumer electronics. Nowadays, it is not uncommon to have a consumer device embedded with wireless power transfer capabilities. Such devices range from electric vehicles to IOT devices and include smartphones, smartwatches, laptops and many more. In fact, being able to power or charge a device without the need of cable is a feature that is very convenient in many aspects especially for applications like IOT wireless power sensors where the use of cables is impractical such as medical implanted devices[3, 4, 5, 6]. It is also the revolution that will drive the electrical vehicles adoption through dynamic charging [7, 8, 9]. The WPT market was valued at 5 billion dollars in 2020 and will reach 35 billion dollars in 2030 with an annual growth of more than 20% [10]. [10] suggests that the near-field WPT which requires a short distance between the transmitter and the receiver (few cm) will still dominate the market. However, most available WPT solutions are limited in terms of range. In order to compensate for that, WPT transmitters have been designed to cover a larger area but they require a complex mechanism and are costly. Therefore, the parallel line feeder transmitter have been introduced as an alternative [11]. Nevertheless, preliminary studies show that the PLF suffers from power fluctuations according to the receiver's position with hinders its practicality. Having a practical WPT transmitter which is intrinsically long enough as the PLF is beneficial in terms of design and cost-effectiveness and could definitely speed up the WPT adoption.

1.2 Statement of the problem

Wireless power transfer (WPT) market is growing fast and many consumers devices are taking advantage of. For most devices such as smartphones, tablets and smartwatches, the wireless charging capability is more like a feature added in complement to the wired charging. However, WPT is a must for sensor network applications when battery replacement is impractical [12, 13, 14, 15, 16, 17, 18].

There are two main WPT technologies, the far-field and the near-field. The far-field is capable of transmitting power over a large distance (in the order of kilometers) and one of it technique is the microwave power transfer (MPT) [19, 20]. It is a radiative type of energy transmission and is suitable for charging low power requirements sensors (∼mW) [21, 22, 23, 24]. The near-field WPT is a non-radiative type of energy transmission which operates with the transmitter and the receiver in a short range (few centimeters). In the near-field scope, the inductive power transfer (IPT) [25, 26] which works similarly to a transformer is the most used techniques. In fact, due to the shorter distance between the transmitter and the receiver, the coupling is strong and can deliver up to watts (W) of power. For some applications, this short range is not sufficient and needs to be extended in order to cover a much wider area. This is the case for sensors networks that require power far beyond the charging capability of the MPT technique but can not afford to have a single transmitter or each sensor in the network. Fortunately, a well-designed IPT transmitting coil could be extended to a wider area. This extension could be achieved by elongating the transmitting coil as in [25, 27] or by deploying many small coils in an array as in [28, 29, 30, 31, 32]. The coil-array technique is capable of selectively focusing the magnetic field toward the receiver in order to create a more efficient coupling. However, this requires a complex mechanism in order to find the receiver position and switch on and/or off the coil directly powering it. However, the elongated-coil design has a much simpler hardware but suffers from an insufficient coupling due to the imbalance in dimensions of the coils. In order for the elongated-coil to become practical, that weak coupling need to be addressed. For a given coupling coefficient, the efficiency of IPT can be improved by increasing the Q-factors of the coils [33, 34, 35, 36]. As the Q-factors can be improved by properly increasing the operation frequency,the parallel line feeder (PLF) system in [11] operates in the 13.56 MHz band, which is higher than the kHz band adopted by many typical IPT systems employing the Qi standard [37]. The PLF in [11] achieves a good theoretical efficiency of about 85% but its coverage is just about 1 m long. Further elongating the feeder makes its length non-negligible compared to the signal wavelength (about 20 m). This results in fluctuation in output voltage according to receiver position due to the standing wave effect.

To address this problem, our preliminary works [38, 39] focused on dividing the PLF into individually resonated segments. But that investigations did not take into account the losses in the feeder which is significantly long relative to the wavelength of its input signal. Therefore, this research considers a PLF modeled as a lossy transmission line [40] to comprehensively define its performance in terms of maximum achievable efficiency.

1.3 Research contribution

The contributions is the dissertation are related to the mitigation of the standing wave occuring in the inductive power transfer system using parallel line feeders. The first contribution make use of wireless communication technique of multiple-input multiple-output (MIMO) scheme for the parallel line feeders in order to benefit from the diversity and multiplexing effects of multiple parallel lines. This help to successfully mitigate the standing wave effect by for higher and stable output power. That first contribution is related to publication (I1).

But, it has been realized that the employment of multiple parallel lines feeders increases the cost of the system which defeats the purpose of our first interest for the PLF.

Also, the efficiency of that first scheme is quite low due to severe dielectric loss caused by the exposure of electric field to the surrounding materials. Therefore, as an improvement, another scheme consisting of a parallel line feeders divided into several resonant segments concatenated together has been evaluated. This segmentation meets the requirements about the length of a line which should be kept under about one-tenth of the signal wavelength to avoid the impact of the standing wave [41, 42]. The result of this scheme is a near-uniform magnetic field strength. Furthermore, this scheme significantly helps reducing the dielectric loss by only exposing the magnetic field. Consequently, this new scheme is shown to be capable of mitigating the standing wave issue while improving the efficiency which makes it more practical for dynamic charging applications. The results of this scheme has also been disclosed in publications (D2) and (I2).
The next contribution could be divided into two sub-contributions:

- The definition of the segmented parallel line feeder theoretical upper-bound efficiency. In that topic, the researcher models the PLF as a lossy transmission line in order to define its maximum achievable efficiency derived from the extended k-Q product formula and shows that a well-designed and uniform segmentation of PLF improves and stabilizes the power efficiency.

- The experimental setup with different configurations of the PLF to confirm the theoretical analysis. In fact, a setup with 5m long PLF at 27.12 MHz

shows that when we can stabilize the efficiency as fairly high practical value for all receiver positions along the feeder.

These contributions have been published in (J1)

1.4 Scope and limitation

The scope of this research includes the design of a parallel line feeder and the definition of its theoretical maximum achievable efficiency. The research is limited and does not include an implementation with a circuit design, impedance matching and/or filtering. But is a good approximation of the upper-bound of RF-to-RF efficiency. It is also taking into account a single transmitter and single receiver setup. However, a single transmitter is long enough to prove the practicality of the system and with its self-contained segments with uniform distributed magnetic field, it is assumed that the multi-receiver setup could be achieved without much degradation of the performance.

1.5 Dissertation layout

The dissertation is divided into 4 chapters. Chapter 1 presents the introduction that includes the motivations, the statement of the problem, the contributions and the limitations of the research. Chapter 2 introduces the fundamentals of wireless power transfer and introduces the inductive power transfer system with parallel line feeder as well as its main issue of the standing wave. Chapter 3 presents the first method for mitigating the intrinsic issue with the PLF by the use of multiple-input multiple-output (MIMO) techniques. Chapter 4 shows the improvement over the MIMO technique for mitigating the standing wave with less resources with an uniformly distributed magnetic field by segmenting the PLF. Chapter 5 quantitatively shows the impact of the segmentation through the definition of the maximum achievable efficiency for the non-segmented and segmented parallel line feeder. It presents the efficiency improvement and stabilization effects over the non-segmented PLF through experimental results. Finally, Chap. 6 will conclude the dissertation and present its related future research opportunities.

Table 1.1 presents the different chapters and their relationship with the publications list referenced on 79.

Table 1.1: Dissertation chapters with its corresponding publications

	J1	I1	I2	D1	D2
chapter 3		◯		◯	
chapter 4			◯		◯
chapter 5	◯				

2 Wireless Charging Using Parallel Line Feeder

2.1 Overview

Wireless Power Transfer (WPT) is the transmission of the electrical power without the use of wires. It is a very essential and convenient technology for many applications such as in medicine where medical implants located in living organism no more need to be removed just to replace their batteries. Also for delivering power to sensors in remote, submerged and contaminated areas. It is also the technology which is supposed to grow the potential of the electrical vehicle adoption. Nowadays, it is quite common for consumers electronics devices to have embedded wireless power transfer capabilities with quite good efficiency. However, there are challenges in expanding power coverage for the wireless power transfer with current technologies. The parallel line feeder is a new configuration of the WPT transmitter that allows the expansion of the power transfer range with less constraints compared to the conventional methods and will be discussed in the following parts of this chapter.

2.2 Fundamentals of wireless power transfer

2.2.1 History

The beginning of WPT started with Nikola Tesla in 1897 who envisioned to electrically connect the whole earth through energy transmitted in the air without wires [43, 44]. Figue 2.1 shows the tower that was built in order to materialize the idea of providing wireless power to the world. It was supposed to power houses, ships and flying objects. In the 1964, William C. Brown has been able to power a small electric helicopter at a distance of 18 meters for ten continuous hours using microwaves therefore demonstrating the possibility of far-field wireless power transfer [45, 46]. In 1994, a team from the University of La Réunion in France have worked on a prototype to provide a remote bassin of the Reunion Island (Grand Bassin) with power wirelessly [47]. They have been able to transmit

Figure 2.1: Nikola Tesla's Wardenclyffe wireless station [1]

around 800 W of electric power over a distance of 40 m.

2.2.2 Classification of WPT

Figure 2.2 shows the different categories of wireless power transfer based on the techniques. There are mainly two types of wireless power transfer which are far-field and near-field. The far-field characterizes the applications where the transmitter and receiver are separated from a long distance (meters to kilometers). It uses radio-frequency radiation at the microwaves (300MHz to 300GHz) and is mostly used to deliver low power to sensors at long distances [48]. It can be convenient to harvest the power from commonly available communication systems such as the Wi-Fi and mobile networks and satellite signals [49, 50, 51, 52, 53, 54]. Other methods such as infrared light or Laser could be used. However, the safety risks they pose make them not common solution for long distances applications. The near-field characterizes the applications where the transmitter and receiver

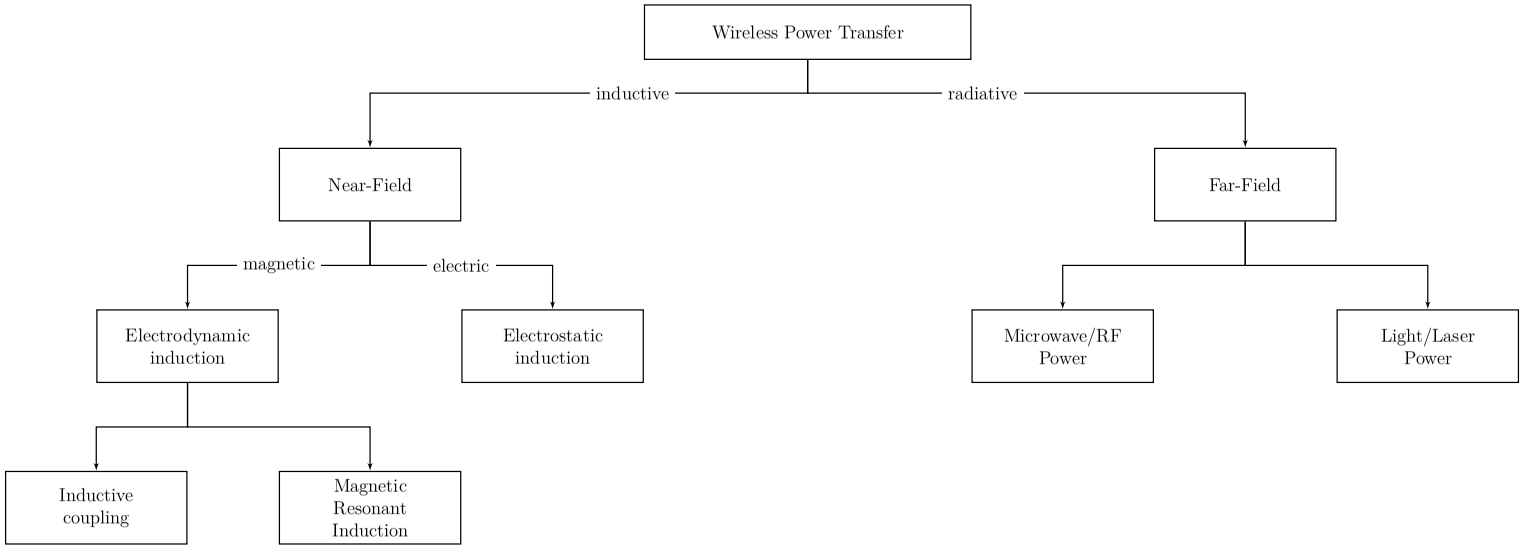

Figure 2.2: Types of WPT

are within few millimeters to centimeters range. For the capacitive coupling, an electric field is created between two electrically conductive electrodes at the transmitter side and could transmit power to a nearby receiver [55, 56, 57]. In this technique, in order to generate sufficient power, the electrodes need to have a great surface which is not always possible with the size of the devices. Another issue is that a large electric field could cause hazard on living organisms and surrounding electronic devices. On the other side, inductive coupling is based on the magnetic induction principle. In fact, a electromotive charge is observed at the end of a coil when it is immersed in a nearby changing magnetic field. That magnetic field could be generated by inserting an alternating current at the port a coil as in Fig. 2.4. The electromotive charge could be rectified and served a generating power at the device load [58]. The magnetic resonant coupling has the same principle with the inductive coupling but additionally create a resonance by adding capacitors to the coil. In fact, working at the resonance, the coupling between the coils is increase for a better energy transfer at greater distance compared to the inductive coupling. In 2007, a group of researchers from the Massachusetts Institute of Technology (MIT) successfully powered a 60-watt light bulb from a distance of 2 meters [59] using the magnetic resonant coupling technique. The electrodynamic induction is the most commonly used in technique of WPT. The applications ranging from radio frequency identification (RFID) systems, medical implants, electrical toothbrushes and shavers, smartphones and tablets to high power demanding electrical vehicles [60, 61, 62, 63, 64, 65, 66].
In this dissertation, we would like to focus on the resonant inductive coupling power transfer.

2.3 Inductive coupling

The inductive coupling is based on Faraday's law of induction which states that whenever a closed circuit is placed in a varying magnetic field, an electromotive force is induced [67, 68]. The electromotive force noted $\mathcal{E}_{21}$ is equal to the negative of the rate of change of the flux linkage Φ_{21} . This emf is :

$$\mathcal{E}_{21} = -\frac{\mathrm{d}\Phi_{21}}{\mathrm{d}t} = -\frac{\mathrm{d}}{dt}\iint_{coil_2} \vec{B_1} \cdot \mathrm{d}\vec{A} \tag{2.1}$$

That rate of change is proportional to the current I_1.

$$\frac{\mathrm{d}\Phi_{21}}{\mathrm{d}t} = M\frac{\mathrm{d}I_1}{\mathrm{d}t} \tag{2.2}$$

That proportionality coefficient M is called mutual inductance and is equal to

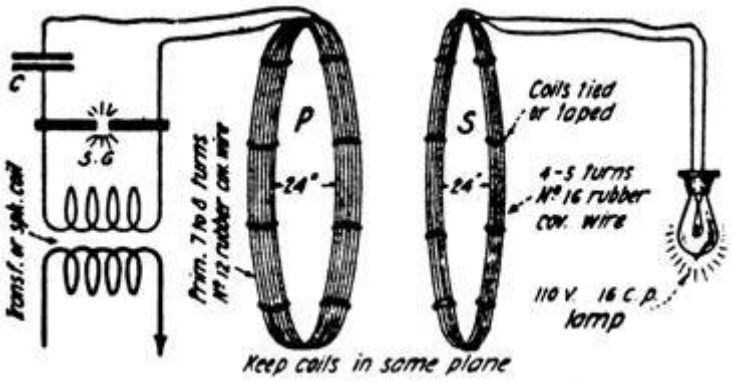

Figure 2.3: Nikola Tesla early prototype of inductive power transfer [2]

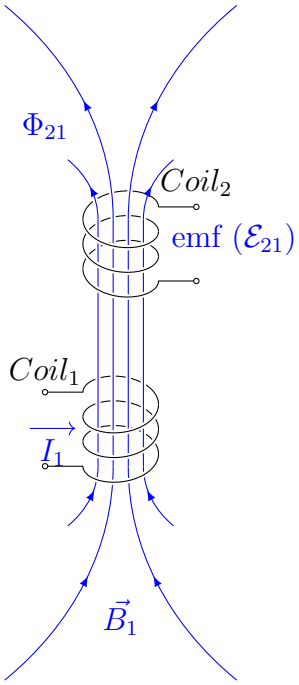

Figure 2.4: Electromagnetic induction

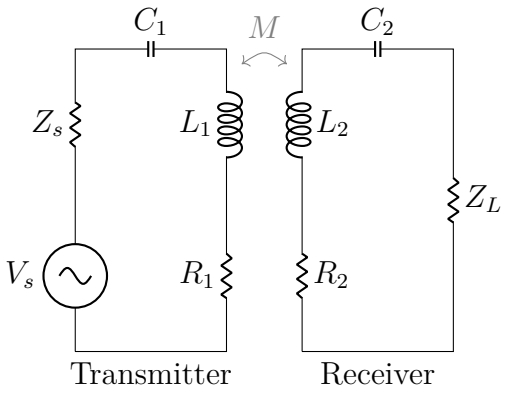

Figure 2.5: Resonant inductive coupling equivalent circuit

the magnetic flux in the $Coil_2$ divided by the exciting current in $Coil_1$.

$$M = \frac{\mathrm{d}\Phi_{21}}{I_1} = \frac{\iint_{coil_2} \vec{B_1} \cdot \mathrm{d}\vec{A}}{I_1} \tag{2.3}$$

Figure 2.3 shows a Nikola Tesla early resonant inductive coupling prototype [2]. An equivalent circuit is presented in Fig.2.5. The driving power could be modeled as an AC source V_s with internal impedance Z_s. The load is modeled as an impedance Z_L. Capacitors C_1 and C_2 are the compensation capacitors in series with L_1 and L_2 respectively. The mutual inductance between the transmitter and receiver is denoted by M.

The coupling coefficient between the two coils noted k is

$$k = \frac{M}{\sqrt{L_1 L_2}} \tag{2.4}$$

$$\tag{2.5}$$

This system could be represented as a 2-port network as in Fig.2.6.

When considering the voltages V_1 and V_2 and the current I_1 and I_2 and their ratio as of

$$Z_{11} = \left.\frac{V_1}{I_1}\right|_{I_2=0} \qquad Z_{12} = \left.\frac{V_1}{I_2}\right|_{I_1=0} \tag{2.6}$$

$$Z_{21} = \left.\frac{V_2}{I_1}\right|_{I_2=0} \qquad Z_{22} = \left.\frac{V_2}{I_2}\right|_{I_1=0} \tag{2.7}$$

$$\tag{2.8}$$

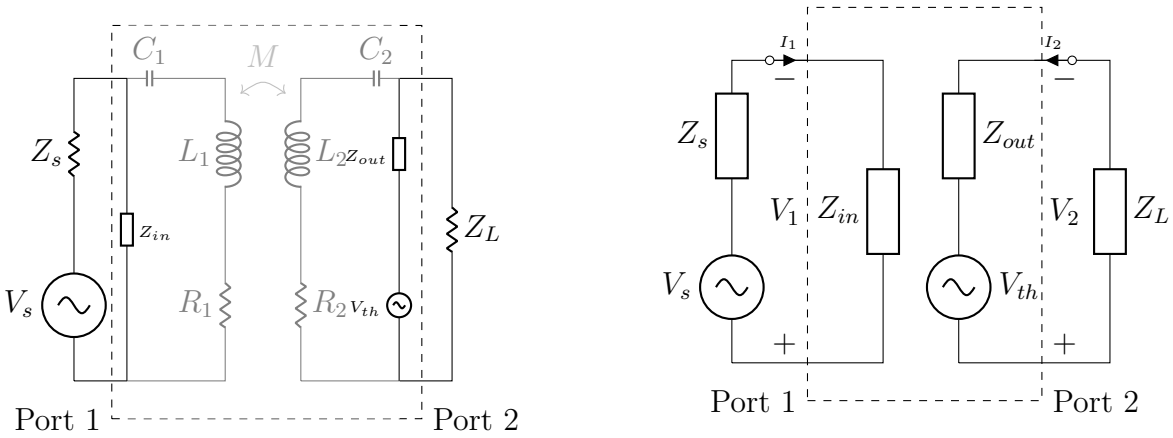

(a) Two port network

(b) Equivalent circuit of the two port network

Figure 2.6: Two port network representation of the inductive coupling system.

we can derive these relations

$$V_1 = Z_{11}I_1 + Z_{12}I_2 \tag{2.9}$$
$$V_2 = Z_{21}I_1 + Z_{22}I_2 \tag{2.10}$$

The impedance parameters Z are

$$\begin{bmatrix} V_1 \\ V_2 \end{bmatrix} = \begin{bmatrix} Z_{11} & Z_{12} \\ Z_{21} & Z_{22} \end{bmatrix} \begin{bmatrix} I_1 \\ I_2 \end{bmatrix} \tag{2.11}$$

The overall efficiency of a WPT system mainly comprises 3 components:

1. DC-to-RF conversion efficiency
2. RF-to-RF transmission efficiency
3. RF-to-DC conversion efficiency

The DC-to-RF efficiency defines how good is the source to propagate the maximum power over the air by reducing losses in its circuitry. The RF-to-RF efficiency determines how the wireless medium is affecting the transmission of the energy and is strongly related to the mutual inductance. The RF-to-DC efficiency at the end defines how the receiver circuit is able to reduce the losses in its circuitry and draw the maximum power at the load.

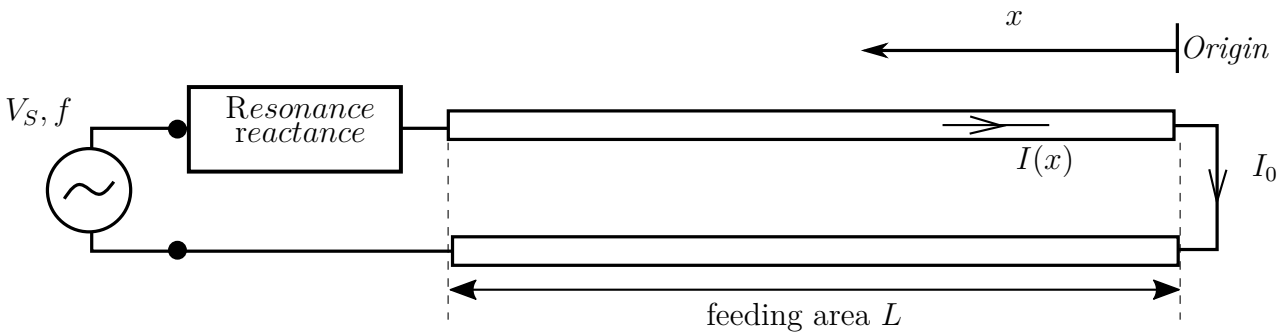

Figure 2.7: Single segment parallel line feeder IPT system configuration.

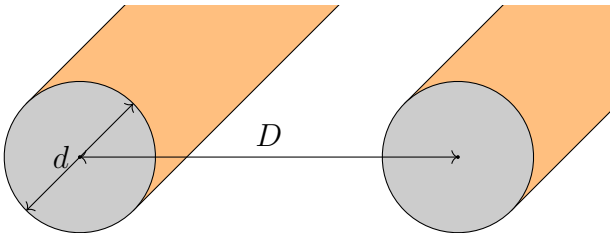

Figure 2.8: Cross section of a PLF.

The DC-to-RF and RF-to-DC efficiencies are quite complex to evaluate since they depend on the source and receiver circuit configuration. We can focus on the RF-to-RF efficiency which can be defined as [69]

$$\eta_{\max} = \frac{k^2 Q_1 Q_2}{(1+\sqrt{1+k^2 Q_1 Q_2})^2} \tag{2.12}$$

where Q_1, Q_2 are the quality factors of the $Coil_1$ and $Coil_2$ respectively with

$$Q = \frac{2\pi f L}{R_{ESR}} \tag{2.13}$$

where R_{ESR} is the series resistance of the coil.
Equation 2.12 shows that the maximum efficiency increases with the increase of the factor $k^2 Q_1 Q_2$.

2.4 Parallel line feeder

Fig. 2.7. shows a general configuration of an inductive power transfer (IPT) system using parallel line feeders (PLF). It consists of two wires placed parallel

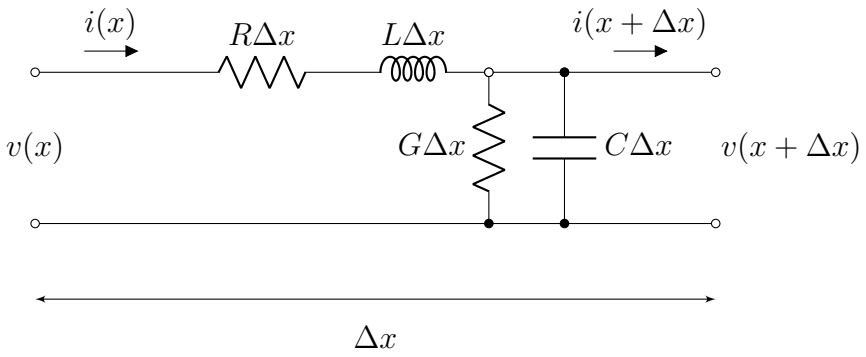

Figure 2.9: Transmission line distributed components.

to each other connected to a sinusoidal RF generator with voltage amplitude V_S, internal impedance R_S, and HF operating frequency f and terminated by a short circuit. The effective feeding area is denoted L. The origin is defined as the end of the line far from the RF generator, therefore for a receiver the position increases while moving away from the end of the line which has position $x = 0$. In order to make the system resonant, the PLF contained a circuit for reactance compensation and resonance.
Since the PLF is operating at a high frequency, it follows the transmission line principle

2.4.1 Transmission line theory

A transmission line can be represented as an infinite series of cascaded two ports networks. A representation of that components could be seen on Fig.2.9. For a small portion of the line Δx, we can assume that the line is composed of a series resistance R, a series inductance L, a capacitance between the two lines C and a conductance of the dielectric separating the two conductors G. The line voltage V(x) and the current I(x) where x is displacement can be expressed in the frequency domain as:

$$\frac{\partial V(x)}{\partial x} = -(R + j\,\omega\,L)\,I(x) \tag{2.14}$$

$$\frac{\partial I(x)}{\partial x} = -(G + j\,\omega\,C)\,V(x) \tag{2.15}$$

which by differentiating gives

$$\frac{\partial^2 V(x)}{\partial x^2} = \gamma^2 V(x) \tag{2.16}$$

$$\frac{\partial^2 I(x)}{\partial x^2} = \gamma^2 I(x) \tag{2.17}$$

where γ is the complex propagation constant and is expressed as

$$\gamma = \sqrt{(R + j\,\omega\,L)(G + j\,\omega\,C)} = \alpha + j\beta \tag{2.18}$$

where α is the attenuation constant and β the phase constant.
The characteristic impedance Z_0 is

$$Z_0 = \sqrt{\frac{R + j\,\omega\,L}{G + j\,\omega\,C}} \tag{2.19}$$

The solutions for $V(x)$ and $I(x)$ are in the form:

$$\begin{aligned} V(x) &= V_{(+)}e^{-\gamma\,x} + V_{(-)}e^{+\gamma\,x} \\ I(x) &= I_{(+)}e^{-\gamma\,x} - I_{(-)}e^{+\gamma\,x} \\ &= \frac{1}{Z_0}\left(V_{(+)}e^{-\gamma\,x} - V_{(-)}e^{+\gamma\,x}\right) \end{aligned} \tag{2.20}$$

$V_{(+)}$ denotes the incident voltage and $V_{(-)}$ the reflected voltage at the load end of the line. Similarly $I_{(+)}$ denotes the incident current and $I_{(-)}$ the reflected current at the load end of the line.

Γ is the reflection coefficient of at the load.

$$\Gamma = \frac{V^-}{V^+} = -\frac{I^-}{I^+} \tag{2.21}$$

Therefore Eq(2.20) becomes

$$\begin{aligned} V(x) &= V_{(+)}\left(e^{-\gamma\,x} + \Gamma e^{+\gamma\,x}\right) \\ I(x) &= \frac{1}{Z_0}\left(V_{(+)}e^{-\gamma\,x} - \Gamma e^{+\gamma\,x}\right) \end{aligned} \tag{2.22}$$

Given the load impedance Z_L,

$$\Gamma = \frac{Z_L - Z_0}{Z_L + Z_0} \tag{2.23}$$

The input impedance Z_{in} of line at a given position x from the load impedance Z_L can be defined as:

$$Z_{\text{in}}(x) = \frac{V(x)}{I(x)} = Z_0 \frac{1 + \Gamma_{\text{L}} e^{-2\gamma x}}{1 - \Gamma_{\text{L}} e^{-2\gamma x}} \tag{2.24}$$

$$Z_{\text{in}}(x) = Z_0 \, \frac{Z_{\text{L}} + Z_0 \tanh(\gamma x)}{Z_0 + Z_{\text{L}} \tanh(\gamma x)} \tag{2.25}$$

For special case where the transmission line is lossless ($\alpha = 0$), the propagation constant becomes purely imaginary ($\gamma = j\beta$). There Eq.()2.25) becomes

$$Z_{\text{in}}(x) = Z_0 \frac{Z_{\text{L}} + j\, Z_0 \tan(\beta x)}{Z_0 + j\, Z_{\text{L}} \tan(\beta x)} \tag{2.26}$$

There are special cases for the transmission line where it is an open circuit ($Z_L = \infty$) and where it is a short circuit ($Z_L = 0$).

	Open circuit $Z_L = \infty$		Open circuit $Z_L = 0$	
	Lossy	Lossless	Lossy	Losseless
$Z_{\text{in}}(x)$	$Z_0 \coth(\gamma x)$	$-j\, Z_0 \cot(\beta x)$	$Z_0 \tanh(\gamma x)$	$jZ_0 \tan(\beta x)$
Γ	$+1$		-1	

Due to the fact that the reflection coefficient is maximum in this special cases, the reflected waves will bounce back to the source as reflected waves. The superposition of the incident and reflected wave creates a standing wave all along the transmission line [40]. In the short-circuit case, as shown in Fig. 2.10a., node where the current is zero happens at the point quarter-wavelength from the end of the line and repeat in a half-wavelength pattern. The voltage node happens immediately at the end of the line since $V_L = 0$ and repeat in a half-wavelength pattern too. In the open-circuit case, the node where the voltage is zero happens at $\lambda/4$ and the current node at the end of the line as shown in Fig. 2.10b. Meaning that the current nodes happen at the voltage antinodes and the current antinodes at the voltage nodes in both cases. Since a open-circuit or a short-circuit

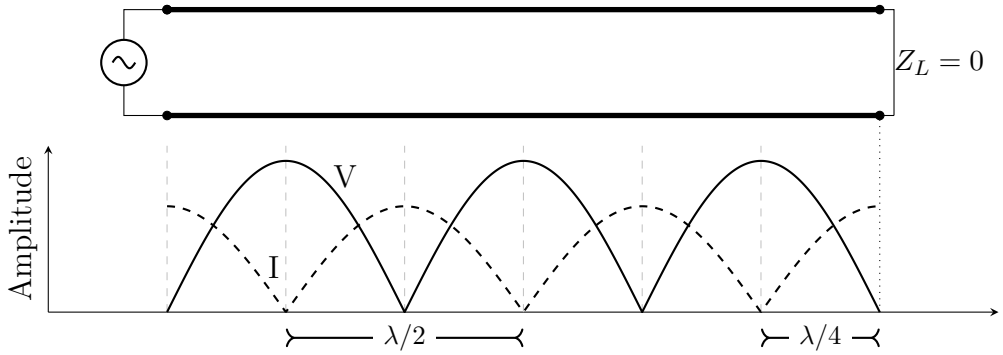

(a) Short-circuit

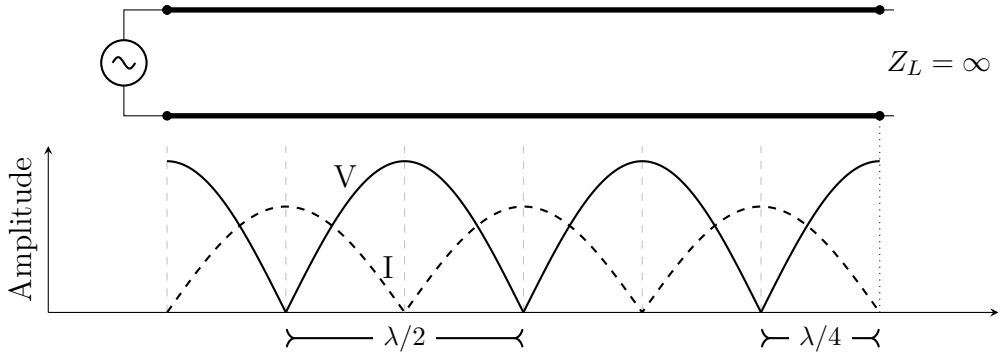

(b) Open-circuit

Figure 2.10: Simple representation of the voltage and current standing wave patterns for open-circuit and short-circuit transmission lines.

transmission line could serve for the PLF, the following investigations exclusively use the parallel line feeder as a short-circuit transmission line.

2.4.2 Standing wave effect on PLF

As aforementioned, the PLF as a transmission line terminated by a short circuit will exhibit a standing wave pattern all over its feeding line. Figure 2.11., shows the pattern of the current measure all over the line. The incident and reflected current waves interfere each other and form a current standing wave pattern along the line. The standing wave is an alternating pattern of nodes, where the current is zero, and anti-nodes,where the current becomes the maximum. Two adjacent nodes and anti-nodes are separated by $\lambda/2$; λ representing the wavelength. Figure 2.12 illustrates an example of the effect of the standing wave from the magnetic field strength representation. One can clearly see the nodes

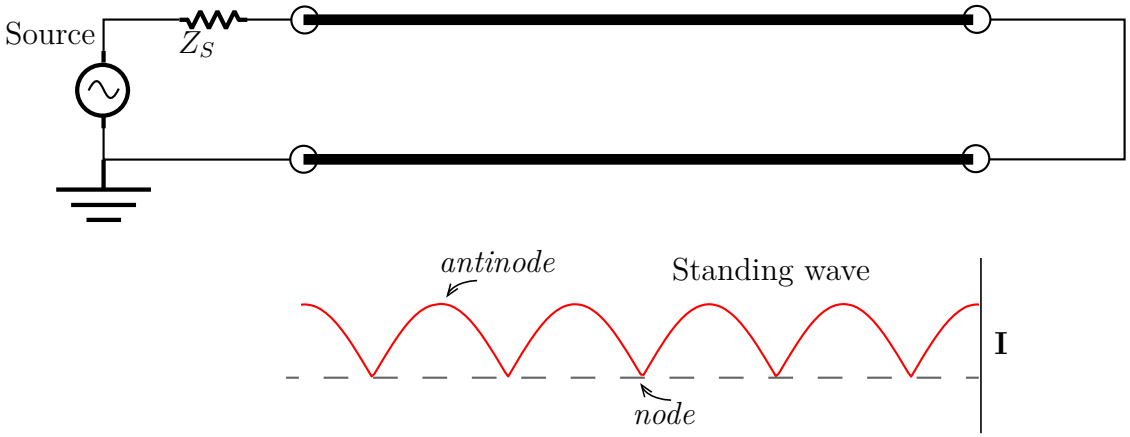

Figure 2.11: Standing wave pattern on a transmission line.

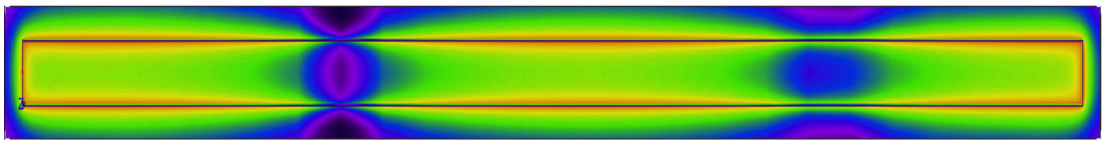

Figure 2.12: Example of standing wave effect in the magnetic field of a parallel line feeder IPT.

and antinodes from that representation. This standing wave effect is not always considered as a drawback and was beneficial for application with the parallel line feeder as a position detection mechanism. In fact, in [70], the standing wave characteristics has been leverage for accurate position detection of tags in an industrial environment. However, regardless of the receiver's configuration and optimization, the PLF power will be fluctuating from a high peak at the antinodes to no power at the nodes. This instability at the transmitter itself is an undesired effect for wireless power transfer applications. Moreover, used as a inductive power transfer system, the fluctuation in the input power of the receiver makes it not practical for commercial applications.

2.5 Summary

In this section, we described the concept of wireless power transfer technology through its history and its different techniques and applications. In this section, we also introduced the parallel line feeder as a new configuration for inductive power transfer applications with the benefits of cost and reduction of maintenance burden. We showed that the fundamentals governing the PLF are derived from

the transmission line theory. However, we discovered that due to the nature of the PLF, it display a standing wave pattern.. Therefore, for the PLF to be deemed practical for commercial applications, the standing wave needs to be mitigated.

3 Parallel Line Feeder with MIMO transmission

3.1 Overview

In the field of inductive coupling, the common usage is *"static"* where the receivers sits on top of the transmitter for the charging. This is the case for applications such as toothbrushes, smartphones and even stationed electric vehicles. These applications work great and are constantly improving in terms of power transfer efficiency and charging time. An example is the Qualcomm Halo™ using magnetic induction to transfer power wirelessly from a transmitter's pad on the ground to a receiver's pad embedded in the vehicle with 90% of efficiency [71]. For the electric vehicles to be immensely adopted, there is the need to be able to charge the vehicles while on the move. In fact, the biggest fear of potential customers of electric cars has even been given a name and is commonly referred as the "range anxiety" [72] [73]. So, as opposed to that static charging, the dynamic charging is the technology that could charge/power a receiver on the move such as a car on the highway. Therefore, the dynamic charging is announced as the key technology for the proliferation of future electric vehicles (EVs) [74]. In fact, as it transfers power inductively from a primary coil buried under the road to pickup coils mounted on the vehicles on the move [75] [76], we can easily imagine electric cars not running out of battery on their way. There are also many benefits for the environment if we could move from the fossil fuels based transportation means to their electric equivalents [77, 78, 79].

For the aforementioned reasons, recently we observe many studies related to dynamic charging. But, despite the high quality and efficiency of actual inductive power transfer systems in terms of static charging, dynamic charging system remains very complex as it involves the motion of the receiver. This motion rapidly changes the inductive power transfer system properties as well as the governing equations.

One of important problems is how to design the transmitting apparatus that is simple and is able to extend its magnetic field coverage in order to charge receivers on the move. In conventional systems as in [80], the primary coil consists of many small coils placed next to each other to cover the feeding area as shown in Fig.3.1a

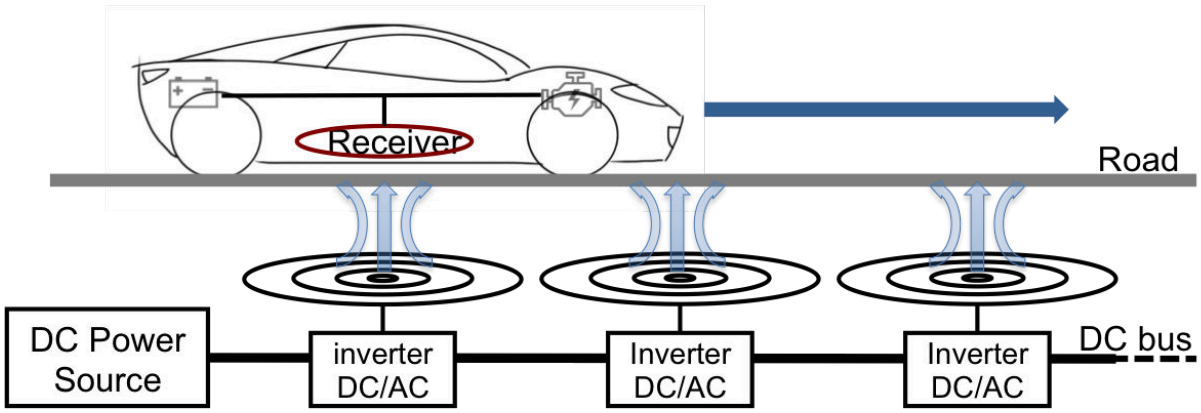

(a) Using coil array.

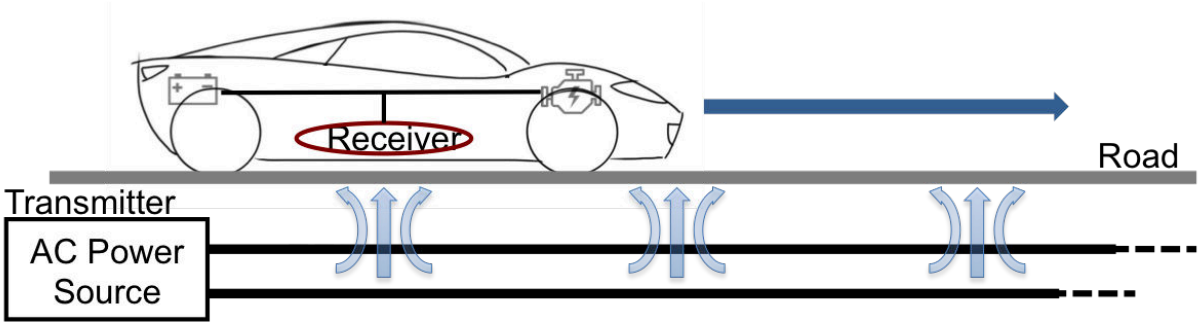

(b) Using parallel line feeders.

Figure 3.1: Different configurations for dynamic charging.

. But, each coil requires an inverter to transform the DC current input into the appropriate output high frequency AC current supply [81] [82] which makes the feeder's circuit more complicated and costly.

Therefore, in [11], authors proposed an elongated parallel line feeder (PLF) which has a large primary structure (Fig.3.1b) which can be easily extendable and cost efficient. This PLF is driven by an HF band (3-30MHz) power supply in order to exploit high resonance coupling for system simplification and misalignment tolerance. However, when the operating frequency is up to several MHz for efficiency enhancement and system simplification, the size of the transmitting apparatus becomes not negligible compared to the wavelength. In such a case, in the unmatched circuit, some of the waves reflect to the source interfering with the incoming ones and eventually yields the standing wave phenomenon on the parallel line feeder. This makes the magnetic field strength fluctuates dynamically along the transmitting apparatus implying that the receiving power is unstable, sometimes falls down to zero and sometimes rises to very high values depending on the position of the receiver's.

Considering that this configuration of the inductive power transfer system is simple enough and cost-effective, it could be promising for practical implementation if that standing wave could be suppressed. A straightforward way of doing so is to insert at the termination of the line an impedance matched to its intrinsic impedance. However, the inserted impedance consumes a lot of power resulting in the power available on the line to become only a very small portion of the input power. This waste reduces the power efficiency. Therefore, this idea is not applicable to the inductive power transfer system using parallel line feeder. The work here will be to find other ways to tackle the standing wave issue.

3.2 Multiple-input multiple-output inductive power transfer using multiple parallel line feeders

The multiple-input multiple-output technique is commonly used in wireless communications where one of its features called diversity technique [83] is especially effective at stabilizing the received signal power against the deviations of attenuation affecting the radio signals. In this proposal, a similar approach has been used as a pattern diversity and is applied by using a configuration where the PLF transmitter (respectively receiver) is the combination of multiple generic PLF (respectively receiver) to transfer stable power to the receiver. Another reason for using multiple feeders is to enhance the output power by utilizing a multiplexing

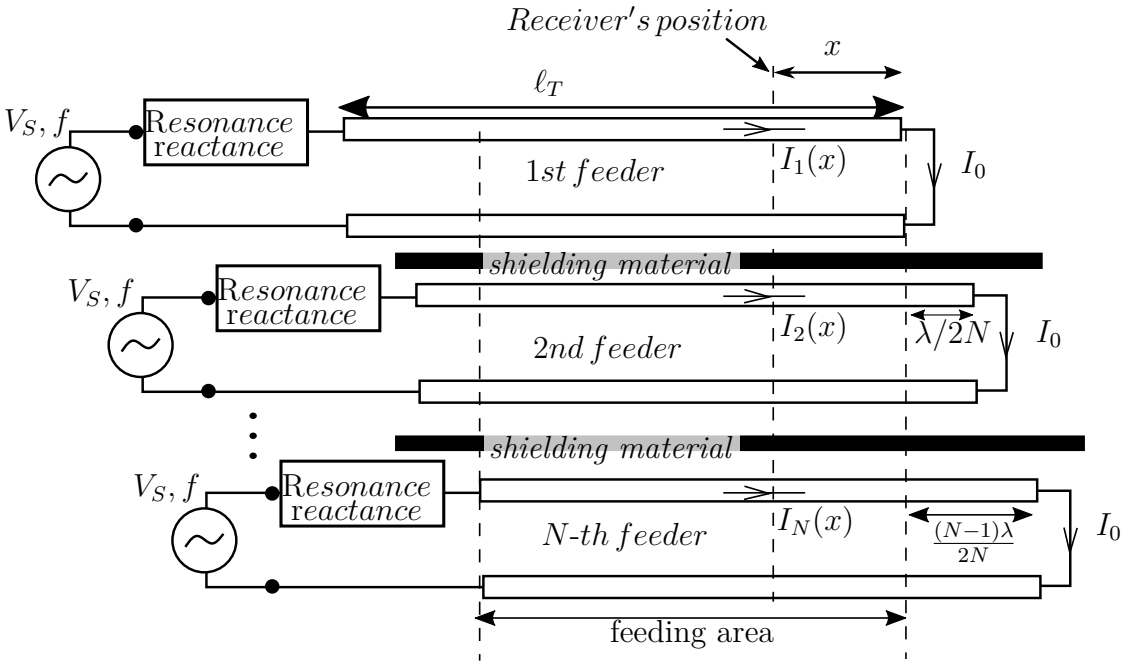

Figure 3.2: Transmitter configuration of an inductive power transfer system using N parallel line feeders.

effect which refers to the significant increase of power resulting from the combination of multiple feeders. But, the multiplication of lines is not enough in order to overcome the standing wave issue. In fact, Fig. 3.3a. presents the wave pattern of 3 non-shifted lines which are difficult to differentiate as their standing wave pattern are overlapping. After the full wave rectification, we could benefit from the increase of amplitude of the combined voltage producing an improvement of the output power at some points but the pattern remains almost the same and we will still face the standing wave problem. For that reason, the parallel line feeders need to be shifted as well in order to get a constant and uniform output power all along the feeding distance. Fig. 3.3b. illustrates that behavior. Also, that way of spreading the overall input power among multiple feeders is important because the input power to each feeder is, definitely, subject to strict limitations to prevent harmful influences to human body as well as to prevent foreign metal objects from being overheated or burned [84].

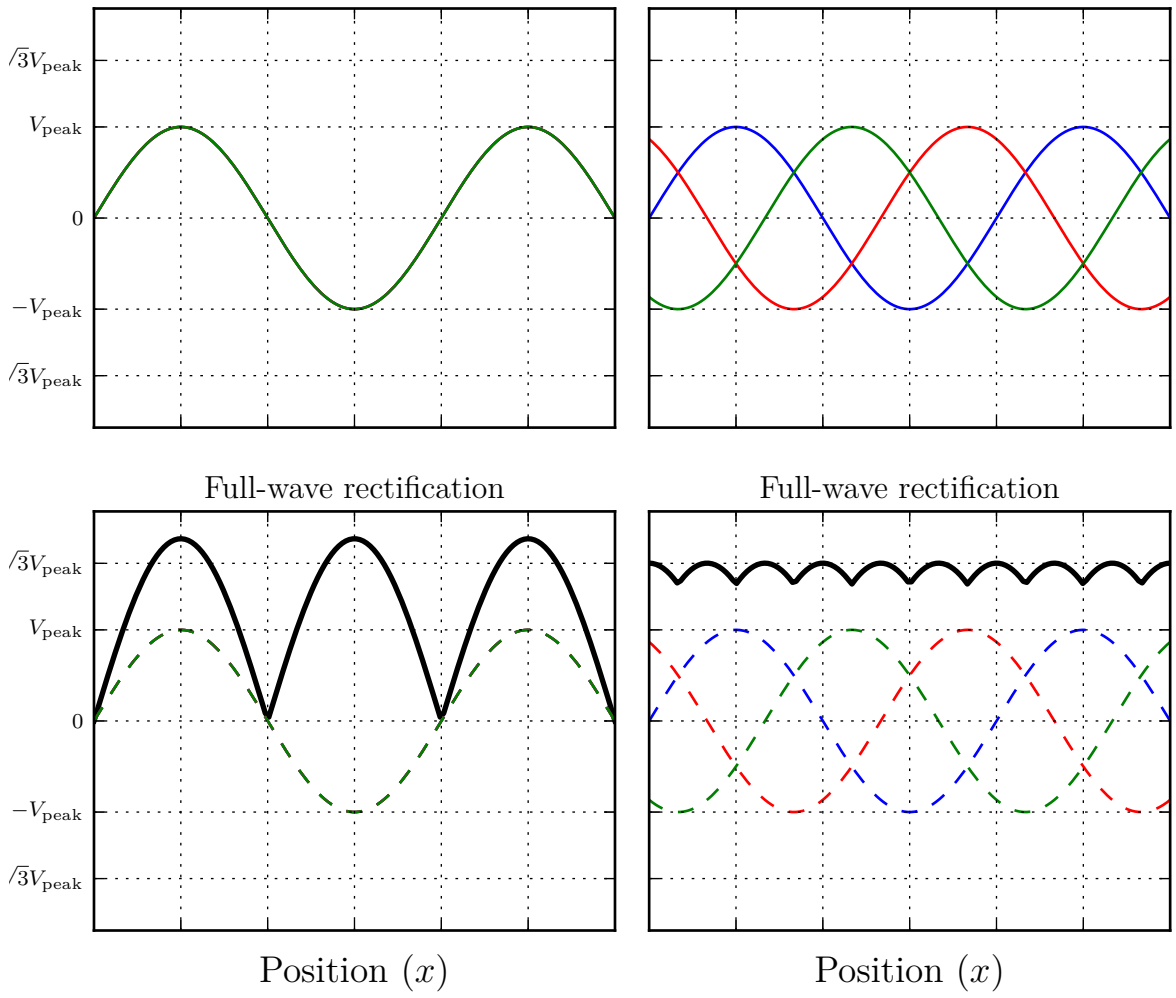

(a) Non-shifted parallel lines feeders.

(b) Shifted parallel lines feeders.

Figure 3.3: Full wave rectification comparison for shifted and non-shifted for N=3. (Full wave rectified output in black)

3.2.1 System model and theoretical analysis

A general transmitter's configuration of the proposed inductive power transfer system using multiple parallel lines is illustrated in Fig. 3.2. N sinusoidal wave generators with identical voltage V_S and frequency f are applied to their corresponding parallel line feeder. Each feeder consisting of two identical wires placed parallel to each other is connected to the source via a tuning reactor to compensate for its reactance and terminated at the other end in a short circuit.

In the case where only one feeder is employed, because of the standing wave, the current expression along the feeder line is

$$I(x) = I_0 \cos \frac{2\pi x}{\lambda}. \tag{3.1}$$

and the receiver at a certain position x from the termination is able to couple the current at that position which is

$$I_S(x) = I_0 \cos \left[\beta \left(x - L\right)\right], \tag{3.2}$$

where $\beta = 2\pi/\lambda$ is the wave number. This shows that the receiver will only pick up the highest power at the anti-nodes but obtains no power at the nodes. Therefore, to mitigate the impact of the standing wave and generating a more evenly distributed magnetic field, multiple feeders are used and shifted in the longitudinal direction by an incremental distance of $\lambda/2N$ where λ is the wavelength. Electromagnetic shielding material is inserted among the feeders to isolate the field of one feeder from those of the others. In such a case, it is a compromise to assume that currents at the terminating ends of the N feeders are identical to I_0.

We assume a receiver is moving on top and along the longitudinal direction. The position of the receiver is denoted by its distance x to the terminating end of the first feeder. Current at location x in the n-th feeder is given by

$$I_n(x) = I_0 \cos \left[\beta x + \left(n - 1\right) \pi/N - \beta \ell_T\right], \tag{3.3}$$

$n \in \{1, ..., N\}$.

The receiver employs N pickup coils to inductively couple and combine power as illustrated in Fig. 3.4. We assume that each pickup only couples with its corresponding feeder, i.e., the n-th couples with the n-th feeder. Thus, each pickup can be viewed as a secondary source with open-circuit voltage

$$V_n^{\text{oc}}(x) = 2\pi f L_{\text{m}} I_n(x), \tag{3.4}$$

where L_{m} is the mutual inductance between the n-th feeder and n-th pickup.

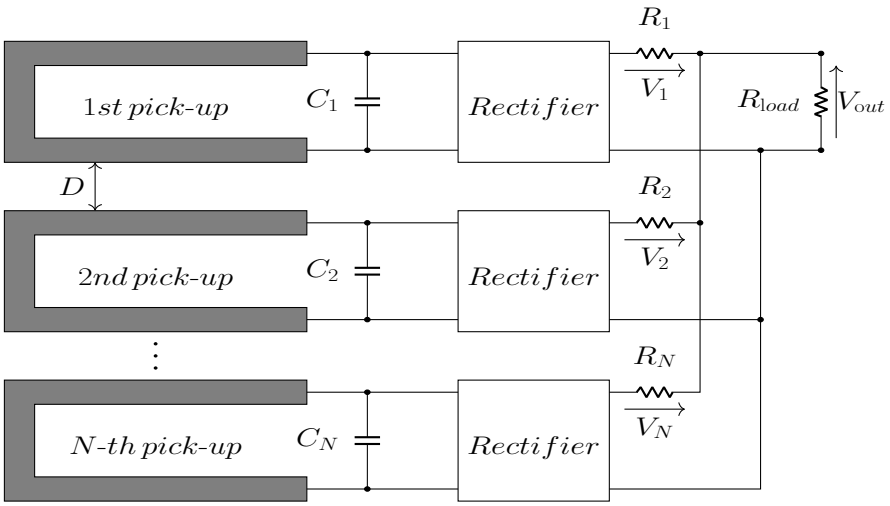

Figure 3.4: Receiver's configuration using N pickups.

Without loss of generality, we assume that the mutual inductances between the feeder and pickups are identical to L_{m}. Similarly, short-circuit current of such a secondary source is given by

$$I_n^{\mathrm{sc}}(x) = L_{\mathrm{m}} I_n(x)/L_2, \tag{3.5}$$

where L_2 is the self inductance of one pickup given that the self inductance of all N pick ups are identical. Therefore, the achievable power that can be drawn from the n-th pickup is $\frac{1}{2}V_n^{oc}(x) \cdot I_n^{sc}(x)$ [25]. To improve the available power, the n-th pickup is parallel tuned by resonant capacitor C_n. If each pickup is perfectly tuned at the operating frequency f, the quality factor of each tuned pickup is determined by its internal resistance and inductance L_2 as well as the operating frequency f. For the sake of simplicity, let Q be the quality factor of each tuned pickup, the available power in each pickup is improved by $2Q$ resulting in

$$P_n(x) = P_0 \cos^2\left[\beta x + (n-1)\,\pi/N - \beta \ell_T\right]. \tag{3.6}$$

Here, $P_0 = \pi Q f I_0^2 L_{\mathrm{m}}^2/L_2$. As shown in (3.6), the available power from the n-th feeder varies with the receiver's position x in a sinusoidal manner with a spatial period of $\lambda/2$. Assuming the receiver is moving with a constant velocity, the average power that the receiver couples after moving a distance of $\lambda/2$ is $P_0/2$.

3.2.2 DC output power

The alternating currents in pickups are rectified to produce direct currents (DC) before being fed in parallel to an single load R_{load}. The load voltage $V_{out}(x)$ monotonically increases with load resistance R_{load}. In the case when R_{load} is small enough such that $V_n^{oc}(x) > V_{out}(x)$ for all $n \in \{1, \ldots, N\}$, the output power is the sum of the available power from all N pickups which is given by

$$\begin{aligned} P_{out}(x) &= \sum_{n=1}^{N} P_n(x) \\ &= P_0 \sum_{n=1}^{N} \cos^2 \left[\beta x + (n-1)\,\pi/N - \beta \ell_T\right] \\ &= \frac{NP_0}{2}. \end{aligned} \tag{3.7}$$

As indicated by (3.7), the output power is, theoretically constant against the receiver's position x showing its stability. Furthermore, the output power is improved by N times compared to the average power of a single feeder.

When R_{load} increases, the load voltage V_{out} increases. As a result, the open-circuit voltage of one or more pickups may be lower than the load voltage V_{out}. In such a case, those pickups do not transfer power to the load, resulting in a lower and more varying output power than that given in (3.7). In the extreme case when the load $R_{load} = \infty$, only the feeder with the highest open-circuit voltage supplies power to the load, resulting in

$$P_{out}(x) = \max_{n \in \{1,\ldots,N\}} \left\{ P_0 \cos^2 \left[\beta x + (n-1)\,\pi/N - \beta \ell_T\right] \right\}. \tag{3.8}$$

The output power profile given in (3.8) is lower and more varying than that the one determined by (3.7). However, this power profile is still higher and more stable than that given in (3.6), which is the output power in the case of single feeder. The stability and improvement of the output power mentioned above demonstrate the diversity and multiplexing effects of the multiple-input multiple-output inductive power transfer system.

3.3 Experiments

3.3.1 Configuration

We conducted experiments to verify the diversity and multiplexing effects of the proposed system with 3 feeders and 3 pickups. In fact, Fig.3.5 shows a typical

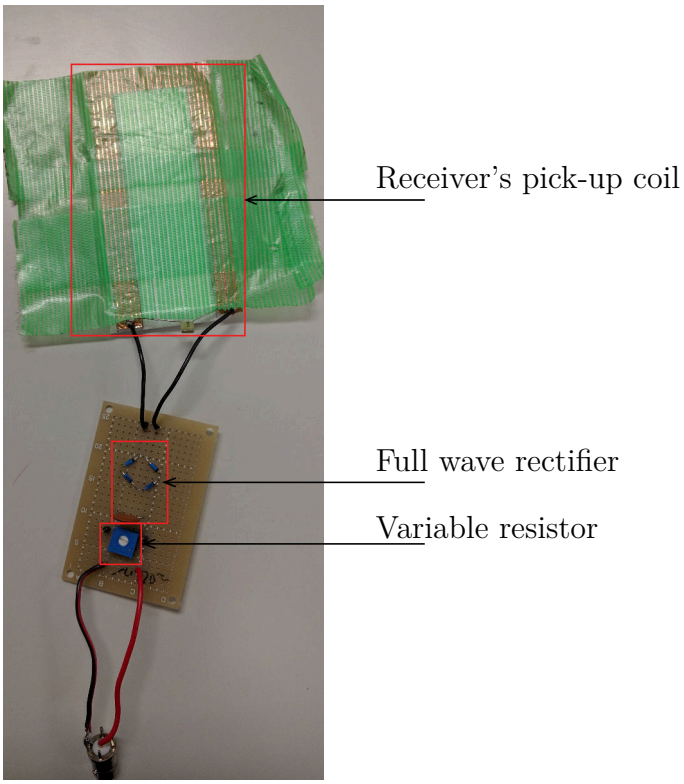

Figure 3.5: Receiver's configuration.

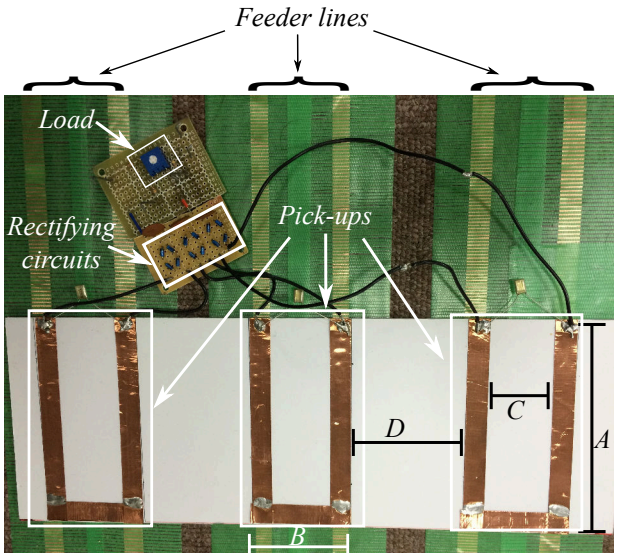

Figure 3.6: Configuration of the experimental system using 3 feeders and 3 pick-ups.

receiver for which couples with a single PLF. In this experimental setup, we combined 3 receivers on top of 3 PLF as illustrated in Fig. 3.6 with parameters given in Tab. 3.1. The voltage measurements for each pickup and the load were performed every meter within the feeding area of 10 m corresponding to the common area shared by the shifted parallel line feeders.

The feeders were powered by 3 HF sinusoidal generators at the frequency f of 13.56 MHz (an ISM band), meaning that the wavelength in vacuum is 22.1 m. However, in the experimental system, a wavelength $\lambda = 16$ m was observed. The feeders were shifted in the longitudinal direction according to the nearest one by a distance of $\lambda/6$ which is practically equal to 2.67 m. Instead of inserting shielding materials among the feeders, we set the distance between two neighboring feeders to a relatively large value $D = 5$ cm to suppress interference among the feeders. At the receiver, each "U" shaped pickup was attached to a full wave rectifying circuit composed with 4 diodes and a smoothing capacitor. Right after, resistances $R_1 = R_2 = ... = R_n = 1\Omega$ were added and their voltages were measured to estimate the currents drawn by the pickups. Then power coupled from each pickup is calculated by using:

$$P_n = V_{out} \times I_n = V_{out} \times \frac{V_n}{R_n}. \tag{3.9}$$

Table 3.1: Experiment parameters

Parameters	**Values**
Operating frequency f	13.56 MHz
Source V_S	7 V
Load impedance R_{load}	50, 100, 200 Ω
Feeding area length	10 m
Air gap between feeders and pickups	2 mm
Pickup configuration A, B, C, D^*	100, 50, 30, 50 mm
Resonance capacitors C_n	1000 pF
Smoothing capacitors of rectifiers	0.1 μF
Diodes for rectifiers	BAT43 (Schottky)

* Dimensions A, B, C, D are illustrated in Fig. 3.6.

At the end, the pickups were connected to the load in order to combine the output power calculated by

$$P_{out} = \frac{V_{out}^2}{R_{load}}, \tag{3.10}$$

where V_{out} is the load voltage.

3.3.2 Results

Fig. 3.7a shows the power drawn by each pickup individually as well as the combined output power when $R_{load} = 100\ \Omega$. The power from the first pickup fluctuated drastically from a high peak value at the anti-nodes corresponding to position $x = 2$ m and $x = 10$ m where the power drawn from the line is maximum, to a very low (almost 0) value at nodes $x = 6$ m and $x = 7$ m where no power could be drawn from the line. This phenomenon is due to the standing wave effect appearing in the current. The amount of power drawn from other pickups follows the same tendency at different positions according to their shifted current standing wave patterns in the longitudinal direction. However, the output power at the load presents a quite stable profile all along the feeding area thanks to the diversity effect as explained in Section 3.2.1. Similar to Fig. 3.7a., a diversity effect is also observed in Fig. 3.7b. and Fig. 3.8a. respectively for $R_{load} = 50\ \Omega$ and $R_{load} = 200\ \Omega$ where the average output power remains quite stable against the fluctuations of the pickups' average power.
Furthermore, Fig. 3.8b. shows the average power of pickups together with the

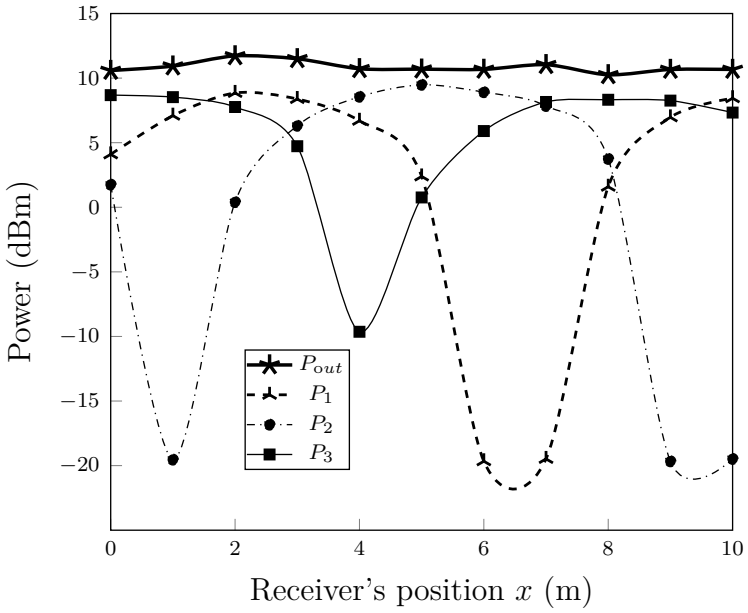

(a) Output power profile when $R_{load} = 100\ \Omega$.

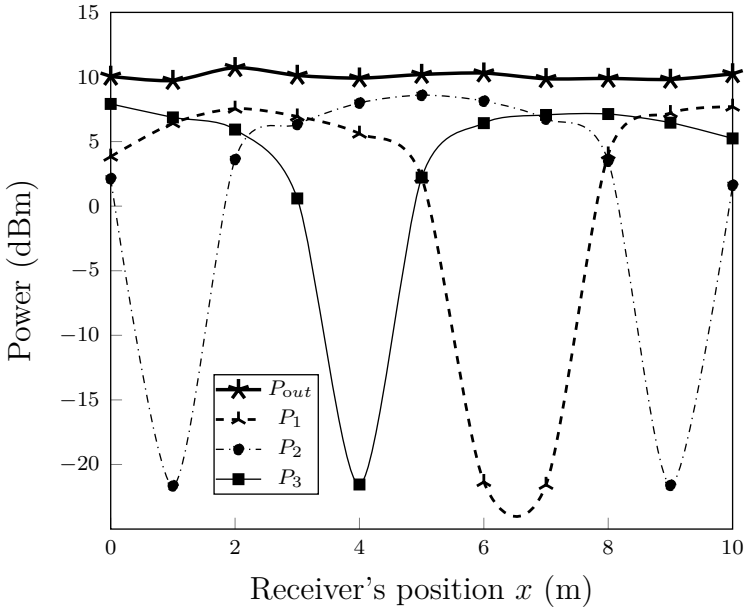

(b) Output power profile when $R_{load} = 50\ \Omega$.

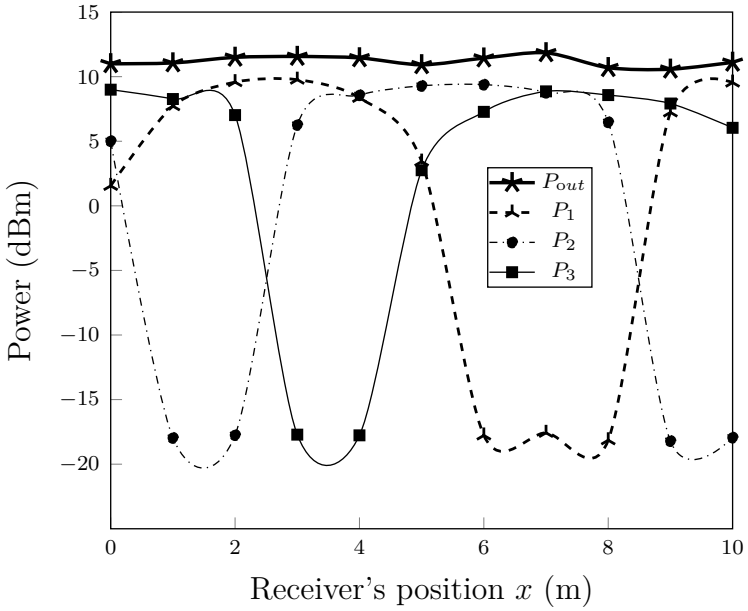

(a) Output power profile when $R_{load} = 200\ \Omega$.

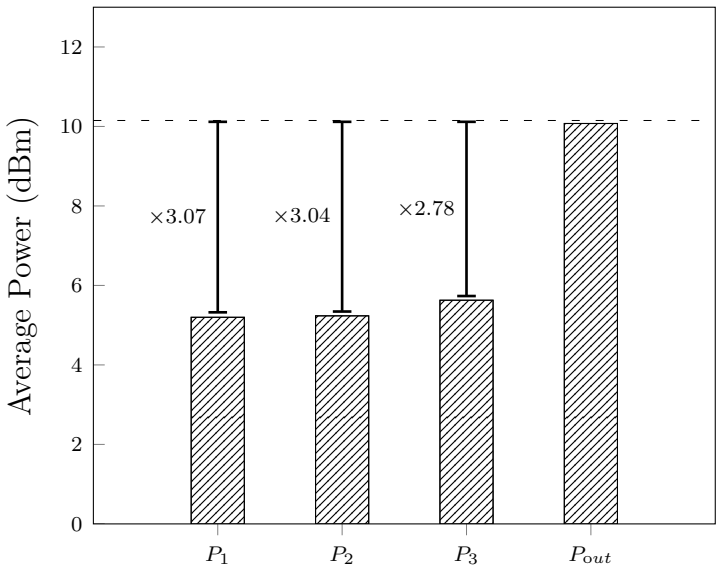

(b) Average power of pickups and load when $R_{load} = 100\ \Omega$.

average output power when $R_{load} = 100\,\Omega$. We can notice that the average output power is at least 4.44 dBm greater than the average power of a single pickup which corresponds to a multiplication factor of 2.78. Again, the multiplication factor is about 3.07 compared to the average power of P_1. The same holds for the other values of load and this improvement can be interpreted as the multiplexing effect and is consistent with the analysis in Section 3.2.1.

Therefore, these experimental results verify the effectiveness of the proposed multiple-input multiple-output inductive power transfer system using multiple parallel line feeders.

3.4 Summary

In this chapter, we evaluated a multiple-input multiple-output inductive power transfer system using multiple parallel line feeders for mitigating the output power variation due to standing wave.
Theoretical analysis and experiments confirmed that the proposed system, exploiting the diversity and multiplexing effects, is capable of overcoming the standing wave issue exposing a stable combined power and also significantly improves the output power compared to the single parallel line case. However, despite these improvements, the computed power transfer efficiency of the overall system was discovered to be quite low which makes this proposal not practical enough. Moreover, it has been realized that the use of multiple PLF complicates and adds costs to our implementation contradicting our proposal for a cheaper and easy to maintain IPT solution.

4 Inductive power transfer using multiple concatenated parallel line feeder segments

4.1 System model

Fig. 4.1a. and Fig. 4.1b. present the configuration and the equivalent circuit of an inductive power transfer system using multiple concatenated PLF segments. In order to combat the impact of the standing wave within one PLF segment, the length of the segment l has been chosen as shorter than one-tenth of a wavelength of the input signal frequency. Each segment is compensated by resonant capacitors C_1 and concatenated to next one.

As the feeder is terminated in a short-circuit, the last segment becomes a short-circuit itself and acts as an inductor with inductance denoted L_1 and is series tuned with two capacitors C_1 following the condition below

$$C_1 = \frac{2}{2\pi f L_1}. \tag{4.1}$$

Consequently, the two-wire line of the previous segment functions also as an inductor with inductance denoted L_1, which is then compensated by two capacitances C_1 according to (4.1). Therefore, all PLF segments resonate at the operating frequency f. There is a phase shift in the magnetic field at the two ends of each segment. The resonant capacitors is determined to recover these phase shifts, thus the magnetic field generated by the whole primary coil is almost uniform.

$$C_2 = \frac{1}{2\pi f L_1}. \tag{4.2}$$

According to [25] , because the secondary coil which is series tuned places a purely resistive impedance R_equ onto the segment right beneath.

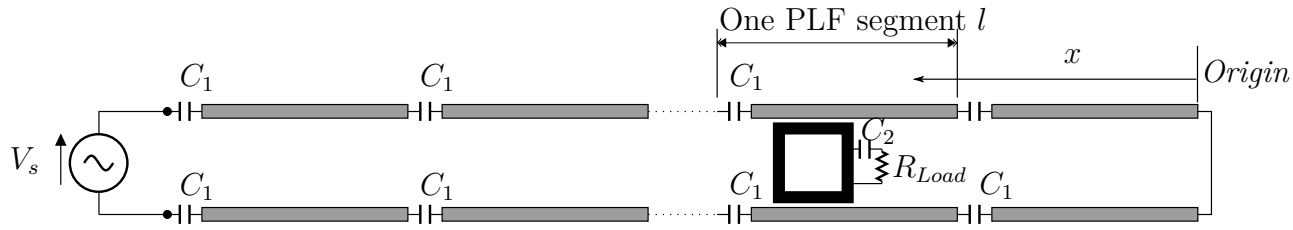

(a) Structure.

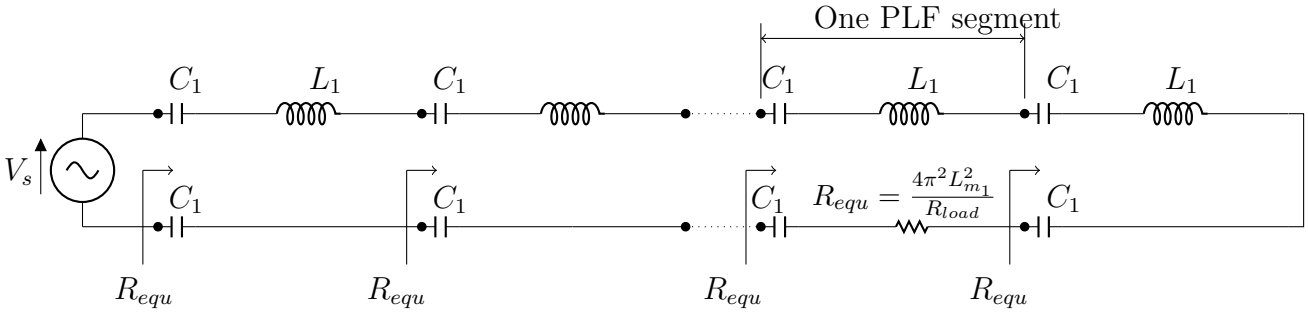

(b) Equivalent circuit .

Figure 4.1: Configuration of an IPT using concatenated PLF segments.

Table 4.1: Simulation parameters

Parameters	**Values**
Operating frequency	$f = 13.56$MHz (ISM band)
Source voltage	$V_S = 1$V
Source's internal impedance	$R_S = 50$
Number of PLF segments	4
PLF segment length	$l = 2$m
Wire distance of PLF segment	$d = 60$cm
Secondary coil	60cm × 2m single-turn rectangular loop
Material of all wires	Copper conductivity $= 5.8 \times 10^7$S/m
Cross section of all wires	4cm×4cm square
Tuning capacitors for primary coil	4 C_1 = (86pF, 93pF, 93pF, 86pF)[1]
Tuning capacitor for secondary coil	$C_2 = 38$pF
Air gap	60cm

[1] Tuning capacitances for 4 segments are slightly different from each other due to fine adjustment for better resonance.

$$R_{equ} = \frac{4\pi^2 L_m^2}{R_{load}}. \tag{4.3}$$

R_equ does not depend on the position x of the receivers according to (4.3). Therefore, we could assume the output power to be stable

4.2 Numerical analysis

In order to evaluate the proposed IPT system, we firstly run simulattions with a Keysight EEsof EDA's electromagnetic simulation software [85] with parameters given in Tab. 4.1. In this analysis, operating frequency $f = 13.56$MHz, an industrial scientific and medical (ISM) band whose wavelength λ is about 22.1m. We analyze a system with 8m long primary coil, consisting of 4 PLF segments, each 2m long. This overall length of the segmented PLF coil is greater than a quarter-wavelength, meaning that the system is sufficient to evaluate the performance under the impact of standing wave.

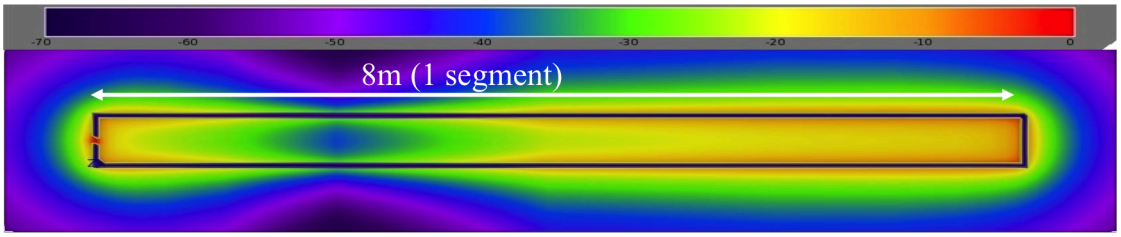

(a) Magnetic field standing wave generated by single PLF segment.

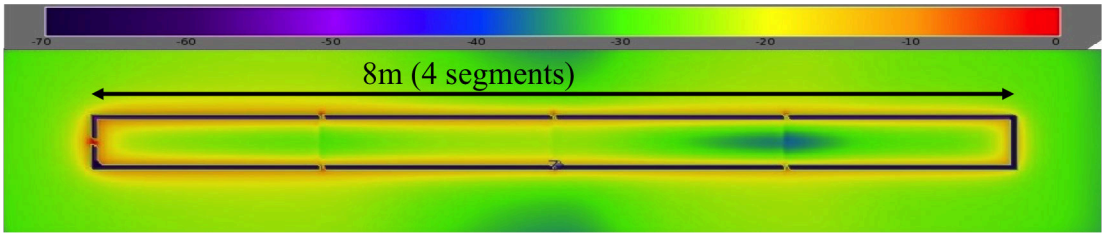

(b) Evenly distributed magnetic field generated by 4 concatenated PLF segments.

Figure 4.2: Comparison of magnetic field distribution between single and multiple segments PLF of 8m long feeding lines.

4.2.1 Magnetic field distribution

The input impedances of 4 segments are as 8.057 + 0.1347j, 4.02 - 2.98j, 2.20 - 0.87j and 0.10 + 0.69j. The very low reactance observed implies that all segments are approximately tuned. As a result, the concatenated 4 PLF segments generate an evenly distributed magnetic field shown in Fig. 4.2b. In the contrary, for the case of a single segment PLF of 8 meters, the magnetic field follows a standing wave pattern demonstrated in Fig. 4.2a.

4.2.2 Output power profile

We investigated the variation of the output power P_{out} consumed at the load R_{load} with receiver's position x. In this investigation, $R_{load} = 50\Omega$ and P_{out} is normalized by $P_{max} = V_S/(4R_S) = 2.5$mW, which is the maximum output power of the source. As demonstrated in Fig. 4.3a., the conventional single segment PLF system shows the dynamically fluctuating power profile characteristic of the standing wave with nulls at x in the 3m, 4m region and standard deviation as large as 0.24. Meanwhile, the proposed multiple concatenated PLF segments method

shows a stable power profile with small standard deviation of 0.07. Furthermore, the smooth variation in output power is also observed even when the receiver moves from one segment to the next.

4.2.3 Input impedance

Figure 4.3b shows the normalized input impedance looking at the source for both the single segment PLF and multiple concatenated segments PLF. The figure indicates a major difference between both PLF configuration. The multiple concatenated segments has an input impedance approximately purely resistive with the resistive component varying slightly in small regions. This result suggests that the proposed scheme is capable of supplying stable output profile without the aid of adaptive tuning circuit.

4.3 Experiments

4.3.1 Configuration

The next step on the segmentation performance assessment was done through experimental evaluation. These evaluations were conducted as a comparison of the performances of the single and multiple segments PLF systems on a quarter wavelength feeding line. The feeders were powered by HF sinusoidal generators at the frequency f of 13.56 MHz (ISM band), which has a wavelength in vacuum of 22.1 m. However, in the experimental system, a wavelength $\lambda = 16m$ was observed. Thus, the feeding area length is set to a quarter-wavelength, which is sufficiently long to evaluate the system performance under the impact of standing wave as done in the numerical analysis. Fig. 4.4. presents the experimental setup. The output power consumed by R_{load} is measured for every 50 cm of the feeding line and use to compute the power transfer efficiency (PTE) of the systems. The experiments' parameters were compiled in Tab. 4.2.

4.3.2 Results

Fig. 4.5b. and Fig. 4.5a. show respectively the power transfer efficiency and the received power profile for different values of R_{load} in single and multiple segments PLF systems. As we can notice in these figures, in the case of single segment PLF system, the output power as well as the PTE drops drastically from a peak value (x=0m) to an extremely low (almost 0) value at the end of the line (x=4m). This is due to the standing wave appearing in the magnetic field. However, in the case

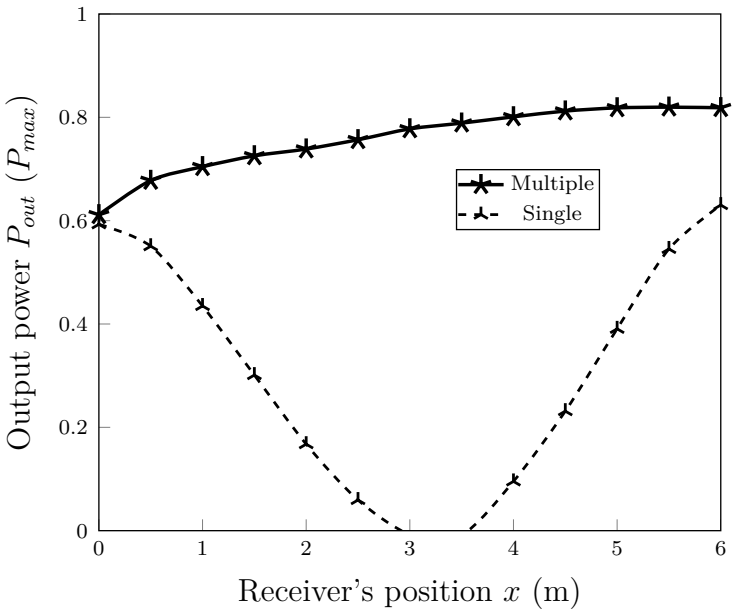

(a) Output power stability for concatenated PLF.

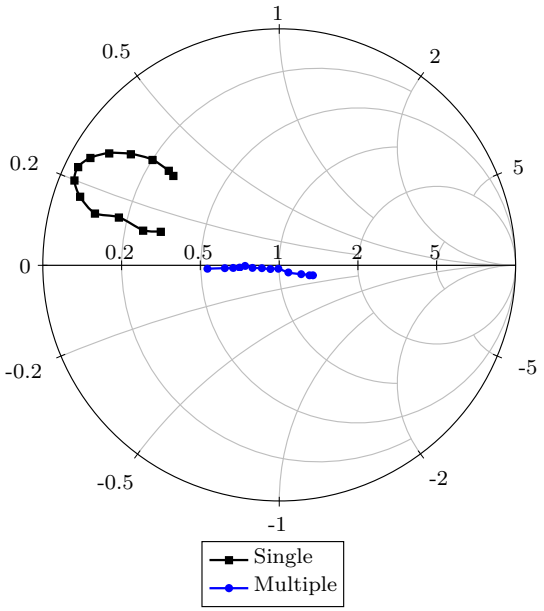

(b) Normalized input impedance of coupled primary coil looked from the source.

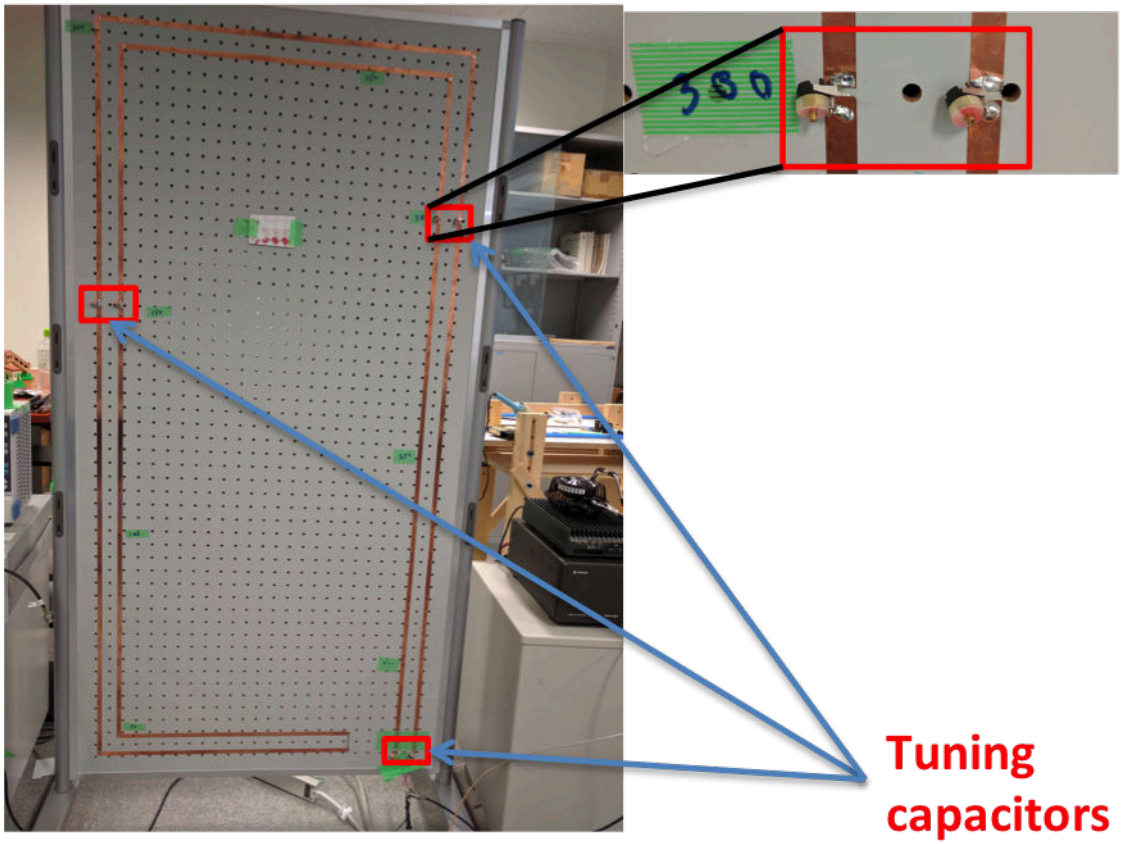

Figure 4.4: Transmitter configuration for a 4 meters IPT system using multiple concatenated PLF.

Table 4.2: Experiments parameters

Parameters	**Values**
Operating frequency	f=13.56 MHz
Load impedance R_{load}	100, 200 Ω
Feeding area length	$\lambda/4 = 4$ m
Air gap	2 mm
Tuning capacitor for C_2	1000 pF

of multiple segments, the output power and the PTE have much greater and a quite stable profile. That demonstrates the better performance of the multiple segments PLF for mitigating the impact of standing wave.

4.4 Summary

The concept of inductive power transfer with multiple self-tuned segments concatenated together with capacitors to form an elongated primary coil have been introduced. The performance comparison between the multiple segment PLF and the single segment PLF was investigated through numerical analysis and simulations. Their results showed that the segmentation effectively helps to mitigate the impact of the standing wave with a uniform magnetic field and increased output power. However, these investigations were limited to the configurations studied only and were considering the PLF as a lossless transmission line. In order for demonstrate the performance of the multiple segments concatenated PLF, a formulation of its characteristics needs to be derived. For practicality reasons, such formulation needs to be complete enough, assuming the PLF as a lossy transmission line.

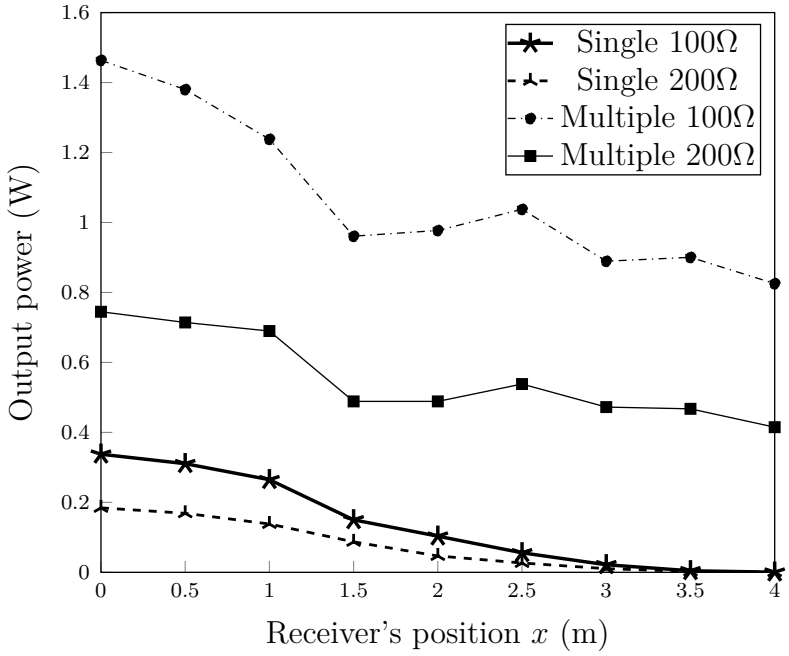

(a) Output power profile for single and multiple concatenated segments PLF system.

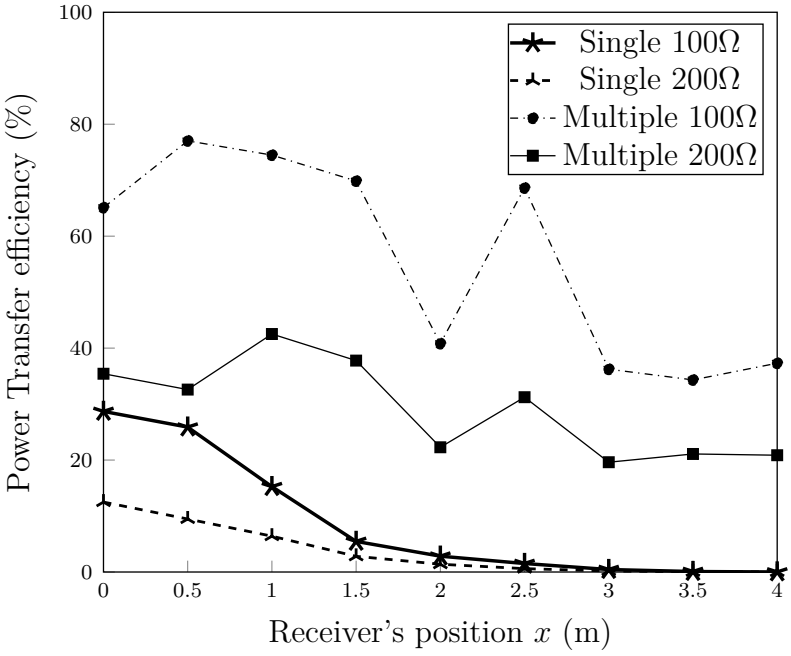

(b) Power transfer efficiency for single and multiple concatenated segments PLF system.

5 Maximum achievable efficiency of the PLF

5.1 Overview

In order to improve the PLF, a segmentation scheme has been adopted which consists in a partitioning of the PLF into smaller segments concatenated together by capacitors. That segmentation scheme is also employed in electrical engineering and called *series compensation* where capacitors are inserted in series in order to increase the transmission system efficiency and stability of long power lines by reducing their impedance, more precisely the inductance of the line [86, 87]. In this research, that segmentation is performed in order to create a more distributed magnetic field in the transmission line. This investigation was performed with two schemes relative to a tenth of the wavelength of the operating frequency ($\lambda/10 = 0.789$ m). A nearly short scheme where each segment is 1 m long and a sufficiently short scheme where the segments are 0.5 m long.

5.2 System model and theoretical analysis of non-segmented PLF

The parallel line feeder consists of a two-wire transmission line of length L is connected to a radio frequency (RF) sinusoidal source via a resonant capacitor C_1 to function as the transmitter coil. Figure 2.8 shows the cross-section of the parallel line feeder with the two parallel wires of identical diameter d separated at a distance D (center-to-center). A simplified schematic of the non-segmented PLF is described in Fig. 5.1(a).

The operating frequency denoted by f is in the MHz range to achieve high Q-factors. The angular frequency is therefore $\omega = 2\pi f$, and the signal wavelength in free space is $\lambda_0 = c/f$, where c is the speed of light. In real applications, the feeder may be surrounded by dielectric materials. In that case, we need to model the PLF as a transmission line with the complex propagation constant $\gamma = \alpha + j\beta$, where α is the attenuation constant and β is the phase constant. The attenuation constant α includes all losses in the feeder, e.g.,copper loss, dielectric

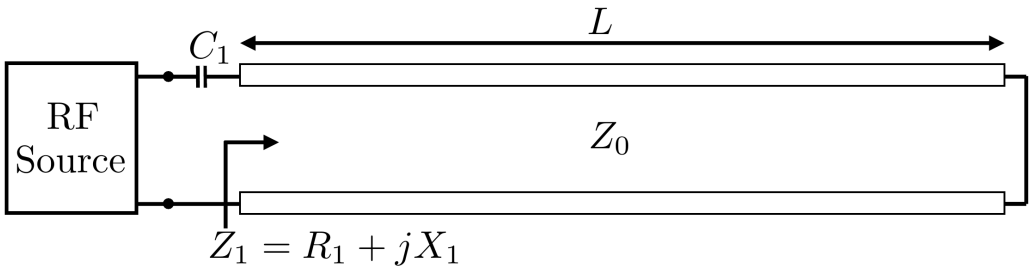

(a) Unloaded condition

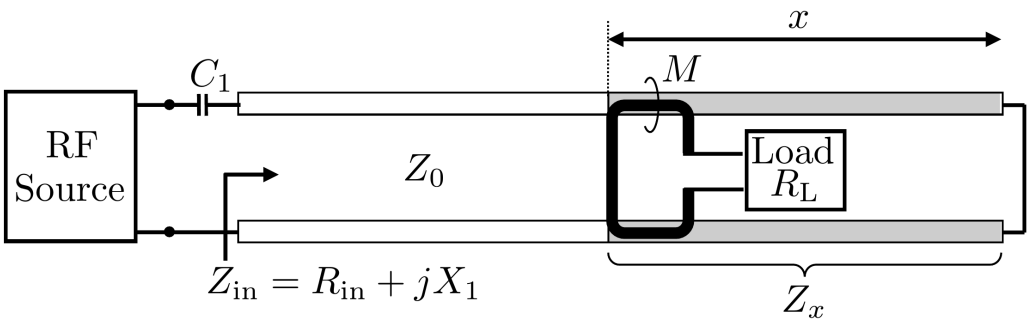

(b) Loaded condition

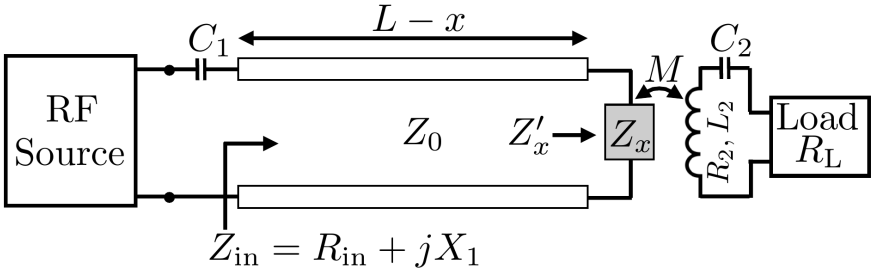

(c) Equivalent circuit of loaded condition

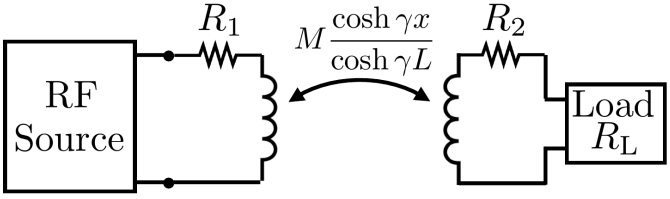

(d) Simplified equivalent circuit of loaded condition

Figure 5.1: System model of a PLF.

loss. From a practical perspective, it is reasonable to assume that the feeder is low loss, meaning that $\alpha L \ll 1$. The phase constant β usually differs from its free space value $\beta_0 = 2\pi/\lambda_0$. Due to the dielectric effect, wavelength of the signal propagated in the feeder is $\lambda = 2\pi/\beta$, which may differ from its free space value λ_0. The ratio of these two values is equal to the refractive index of the dielectric $n = \lambda_0/\lambda$.

The characteristic impedance of the feeder Z_0 [88]

$$Z_0 = \frac{120\,\Omega}{n} \cosh^{-1} \frac{D}{d} \tag{5.1}$$

Without loss of generality, throughout this research we assume that the feeder is terminated in a short circuit. In the unloaded condition in Fig. 5.1(a), the input impedance of the feeder is

$$Z_1 = Z_0 \tanh \gamma L = R_1 + jX_1, \tag{5.2}$$

where

$$R_1 = \frac{Z_0 \sinh(2\alpha L)}{\cosh(2\alpha L) + \cos(2\beta L)} \tag{5.3}$$

$$X_1 = \frac{Z_0 \sin(2\beta L)}{\cosh(2\alpha L) + \cos(2\beta L)} \tag{5.4}$$

In order to achieve the resonance, the imaginary part jX_1 in Eq. (5.5) will be cancelled with its equivalent capacitor $C_1 = 1/(\omega X_1)$ while the real part R_1 remains. Therefore,

$$Z_1 = Z_0 \tanh \gamma L = R_1 \tag{5.5}$$

Now, let us consider the loaded condition illustrated in Fig. 5.1(b) when a receiver is located at the position x from the terminating end of the feeder. In this case, the system has two different parts that need to be analyzed separately. The part of length x on the right-hand side which is coupling with the receiver's coil, and the remaining part of length $L - x$ on the left-hand side which does not couple with the receiver. The coupling part can be seen as a shorted transmission line of length x and therefore its input impedance can be expressed as

$$Z_x = Z_0 \tanh(\gamma x) \tag{5.6}$$

Via the coupling, the load reflects an impedance on the feeder. Let the mutual coupling between the feeder and the receiver coil be M, the internal resistance of

the receiver coil be R_2, then the impedance that the load reflects on the feeder is $\omega^2 M^2/(R_2 + R_L)$ [25, 36]. Equivalently, the non-coupling part of the feeder is terminated in an impedance Z'_x as illustrated in Fig. 5.1(c).

$$Z'_x = Z_0 \tanh(\gamma x) + \frac{\omega^2 M^2}{R_2 + R_L}. \tag{5.7}$$

The input impedance of the loaded feeder is

$$\begin{aligned}
Z_{in} &= Z_0 \frac{Z'_x + Z_0 \tanh[\gamma(L-x)]}{Z_0 + Z'_x \tanh[\gamma(L-x)]} \\
&= Z_0 \frac{\tanh(\gamma x) + \tanh[\gamma(L-x)] + \dfrac{\omega^2 M^2}{Z_0(R_2+R_L)}}{1+\tanh(\gamma x)\tanh[\gamma(L-x)] + \dfrac{\omega^2 M^2}{Z_0(R_2+R_L)}\tanh[\gamma(L-x)]} \\
&= Z_0 \frac{\sinh(\gamma L) + \dfrac{\omega^2 M^2}{Z_0(R_2+R_L)} \cosh(\gamma x)\cosh[\gamma(L-x)]}{\cosh(\gamma L) + \dfrac{\omega^2 M^2}{Z_0(R_2+R_L)} \cosh(\gamma x)\sinh[\gamma(L-x)]} \\
&= Z_0 \tanh(\gamma L) \frac{1 + \dfrac{\omega^2 M^2}{Z_0(R_2+R_L)} \dfrac{\cosh(\gamma x)\cosh[\gamma(L-x)]}{\sinh(\gamma L)}}{1 + \dfrac{\omega^2 M^2}{Z_0(R_2+R_L)} \dfrac{\cosh(\gamma x)\sinh[\gamma(L-x)]}{\cosh(\gamma L)}}
\end{aligned} \tag{5.8}$$

Because, the characteristic impedance Z_0 is usually large compared to the reflected load $\omega^2 M^2/(R_2 + R_L)$, the term $\omega^2 M^2/(Z_0(R_2 + R_L))$ is very small compared to one. Therefore, Z_{in} can be approximated as

$$\begin{aligned}
Z_{in} &\approx Z_0 \tanh(\gamma L) \Bigg\{ 1 + \ldots \\
&\qquad + \frac{\omega^2 M^2 \cosh(\gamma x)}{Z_0(R_2+R_L)} \left[\frac{\cosh[\gamma(L-x)]}{\sinh(\gamma L)} - \frac{\sinh[\gamma(L-x)]}{\cosh(\gamma L)} \right] \Bigg\} \\
&\approx R_1 + \frac{\omega^2 M^2 \dfrac{\cosh^2(\gamma x)}{\cosh^2(\gamma L)}}{R_L + R_2} + jX_1
\end{aligned} \tag{5.9}$$

Obviously, the imaginary part of Z_{in} is equal to that of Z_1 in Eq. (5.5). Therefore, similar to the unloaded feeder, the loaded feeder is also compensated by the same

capacitor C_1. As a result, after compensation the input impedance of loaded feeder is purely resistive

$$Z_{in} = R_{in} \approx R_1 + \frac{\omega^2 M^2 \dfrac{\cosh^2(\gamma x)}{\cosh^2(\gamma L)}}{R_L + R_2}. \tag{5.10}$$

Based on Eq. (5.10), a simplified equivalent circuit for the loaded PLF system is described in Fig. 5.1(d). From this model, the square of kQ-product denoted χ is derived as a function of location x as follows.

$$\begin{aligned}
\chi(x) &\approx \frac{\omega^2 M^2}{R_1 R_2} \left| \frac{\cosh \gamma x}{\cosh \gamma L} \right|^2 \\
&\approx \frac{\omega^2 M^2}{Z_0 R_2} \frac{\cosh(2\alpha L) + \cos(2\beta L)}{\sinh(2\alpha L)} \frac{\cos^2 \beta x}{\cos^2 \beta L} \\
&\approx \frac{\omega^2 M^2}{Z_0 \alpha L R_2} \cos^2 \beta x \\
&\approx \chi_0 \cos^2 \beta x
\end{aligned} \tag{5.11}$$

where χ_0 is a constant against the receiver position x

$$\chi_0 = \frac{\omega^2 M^2}{Z_0 \alpha L R_2} \tag{5.12}$$

The complete efficiency of a WPT system is mostly the combination of three efficiencies:

- DC-to-RF conversion efficiency
- RF-to-RF transmission efficiency
- RF-to-DC conversion efficiency

These efficiencies variate due to some many considerations especially the complex impedance of the load. So, it becomes rather complicated to evaluate them. However, we can focus on the RF-to-RF efficiency assuming that the load impedance is optimized to draw the maximum power according to the Z-parameters of the transceiving apparatuses. We can therefore take advantage of the concept of the maximum achievable efficiency [33]. That maximum achievable efficiency becomes the theoretical upper-bound on the overall efficiency of the whole system, which is related to the kQ-product as follows.

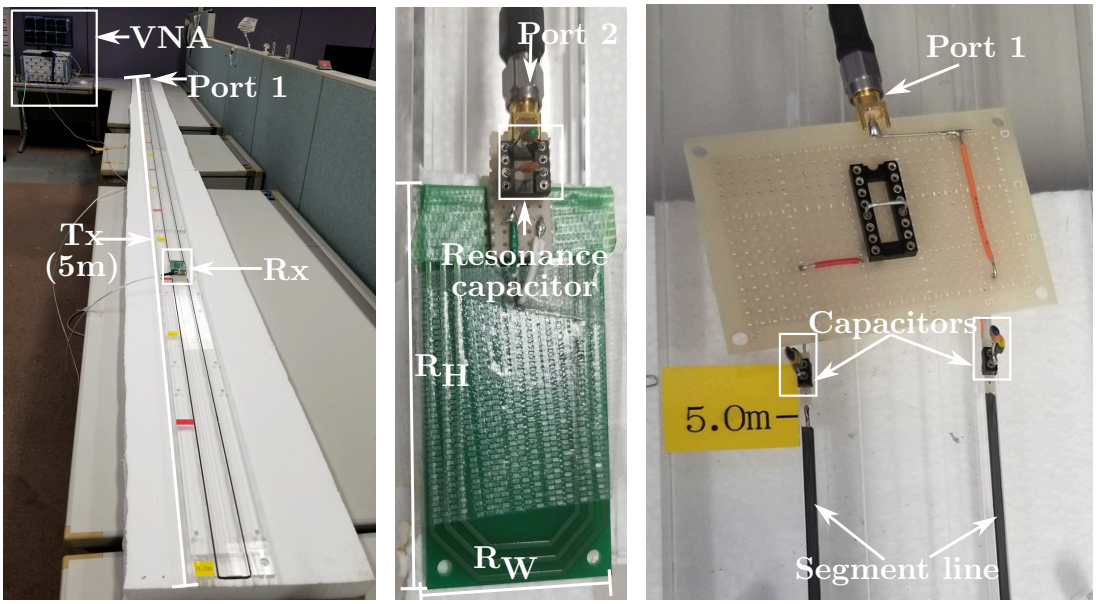

(a) (b) (c)

Figure 5.2: Experimental setup.

$$\eta_{\max}(x) = 1 - \frac{2}{1+\sqrt{1+\chi(x)}} = 1 - \frac{2}{1+\sqrt{1+\chi_0 \cos^2 \beta x}} \tag{5.13}$$

Equation (5.13) shows that the maximum efficiency $\eta_{\max}$ vary drastically with the receiver position x, following a standing wave pattern represented by the term $\cos^2 \beta x$. This equation also implies that not the value of R_1 but the term $Z_0 \alpha L$ represents losses in the feeder.

5.2.1 Experimental results

In order to confirm the theoretical conclusions in Sect. 5.2, experiments were carried out with the configuration of the PLF to the longest that could fit into our experimental environment and also long enough to be non-negligible compared to the wavelength of the input signal. The experimental setup of the overall system is shown in Fig. 5.2(a).

In this figure, the feeder is a two-wire transmission line of length $L = 5$ m and width $D = 40$ mm, built from copper wires of diameter $d = 4$ mm and conductivity of 5.8×10^7 S/m. The feeder is terminated in a short-circuit at one

end. The other end is connected to the resonant capacitors and attached to the port 1 of a vector network analyzer (VNA) R&S©ZNBT8 as in Fig. 5.2(c).

As shown in Fig. 5.2(b), the receiver is a spiral coil embedded in a 4 cm $\times$ 8 cm printed circuit board (PCB) with added capacitors for resonance. The receiver coil is connected to the port 2 of the VNA for measurement. All the port impedances are 50 Ω. The operation frequency $f = 27.12$ MHz has been chosen for the experiments.

In the unloaded condition, the intrinsic values of the internal resistance of the feeder and that of the receiver coil are measured as $R_1 = 58.4\ \Omega$ and $R_2 = 1.4\ \Omega$, respectively. In the loaded condition, the receiver is aligned on top of the feeder and is moved from the right-hand side to the left-hand side toward the source at a step of 25 cm in the x direction. The the air gap between the feeder and the receiver coil is 2 mm. For each position x of the receiver, we measured the Z-parameters (Z_{11}, Z_{12}, Z_{21}, Z_{22}) and calculated the maximum efficiency by using formula given in [32] as follows.

$$\eta_{exp}(x) = 1 - \frac{2}{1 + \sqrt{1 + \dfrac{|Z_{21}(x)|^2}{\mathrm{Re}\{Z_1\}\mathrm{Re}\{Z_2\}}}} \tag{5.14}$$

The measurement results of $\eta_{exp}(x)$ are shown by the square dots in Fig. 5.3. and a fitted curve following Eq. (5.13) for the measurement results. That fitted curve matches very well with the measurements, indicating that the theoretical formula Eq. (5.13) accurately reflects the system properties. Based on the estimated values from the curve which are $\beta = 0.796$ rad/m and the constant $\chi_0 = 14.74$, we can substitute the values of β, χ_0, R_1 and R_2 into Eq. (5.12) to obtain the mutual inductance $M = 134.1$ nH. The wavelength of the signal propagated in the feeder is $\lambda = 2\pi/\beta = 7.89$ m, thus the dielectric of the feeder has a refractive index of $n = 1.4$ and the characteristic impedance of the feeder is $Z_0 = 357.6\ \Omega$. Some other parameters for the PLF system are summarized in Tab. 5.1.

Importantly, Fig. 5.3 shows that the efficiency is not stable all over the feeder length. In fact, it varies drastically based on the receiver position x following a standing wave pattern. We can observe that at the terminating end ($x = 0$) position, the efficiency is at its highest but it starts decreasing when the receiver moves toward the source. Its lowest value, nearly zero is when the receiver is around the position $x = 200$ cm. When moved further toward the source, the efficiency starts to increase again until reaching the peak of approximately 60% near the position $x = 400$ cm. And then it decreases all the way to the source.

Table 5.1: Estimated values of the PLF parameters.

Quantity	Value	
Phase constant β	0.796	[rad/m]
Wavelength $\lambda = 2\pi/\beta$	7.89	[m]
Free-space value of wavelength λ_0	11.05	[m]
Refractive index of dielectric $n = \lambda_0/\lambda$	1.4	
Mutual inductance M	134.1	[nH]
Characteristic impedance $Z_0 = \frac{120\,\Omega}{n} \cosh^{-1} \frac{D}{d}$	357.6	[Ω]

We can easily assume that this pattern is repeated periodically every quarter-wavelength. That drastic variation of efficiency following a standing wave pattern mentioned above limits the deployment of the PLF system as a practical system.

5.3 Summary

Modeling the PLF as a lossy transmission line helped to understand it characteristics especially nature of the losses contributions. The fact that its resistive component is large reduces the transmission efficiency to a great extend making the peak efficiency only around 60%. It helped also defining its maximum achievable efficiency. However, that maximum achievable efficiency as been proved to be following the same standing wave pattern as the previous investigations which makes is concentrating the most power at the current anti-nodes spaced by a quarter-wavelength. So, that configuration of the PLF is not deemed suitable enough for IPT applications.

5.4 System model and theoretical analysis of segmented PLF

This section presents the segmented PLF which is a modification for the PLF to improve and stabilize the power transfer efficiency. The proposed segmented PLF is shown in Fig. 5.4(a), where the feeder of length L is equally divided into N segments, thus each segment having a length of $l = L/N$. The number of total segments N is chosen so that the segment length $l = L/N$ is short. The purpose is to guarantee the magnetic field generated by one segment is even and the

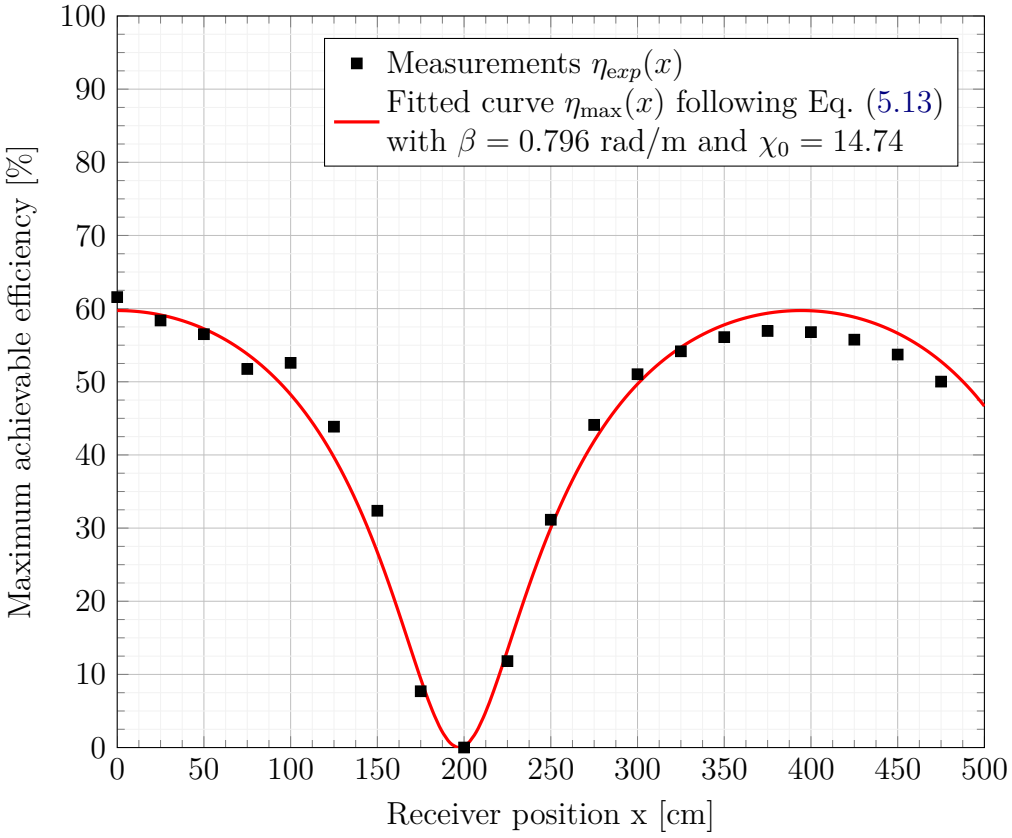

Figure 5.3: Maximum achievable efficiency of PLF system in Fig. 5.2 for air gap of 2mm.

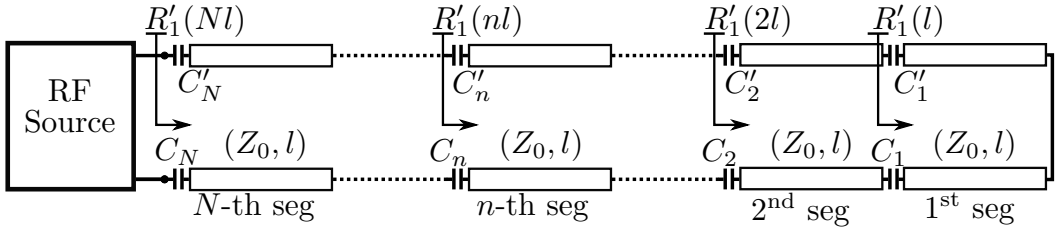

(a) Unloaded condition

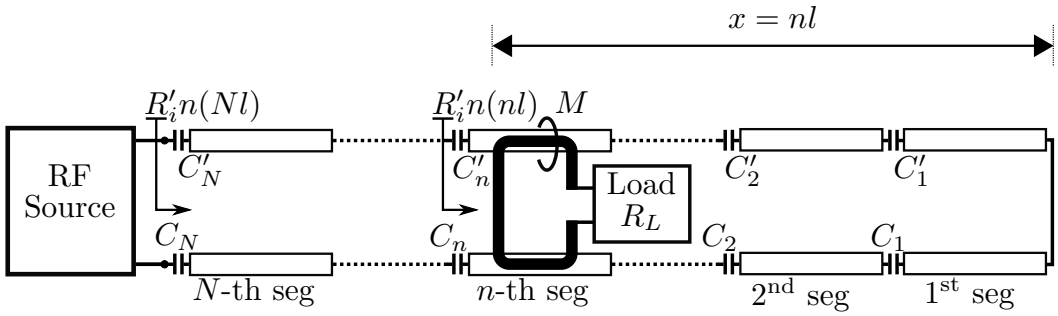

(b) Loaded condition

Figure 5.4: System model of segmented PLF.

system efficiency does not significantly change as the receiver coil moves within one segment. However, due to the physical nature of the segmented PLF, we can expect the system efficiency to vary when the receiver is moving from one segment to another. The segments are numbered as $\#n$, where $n \in \{1, 2, \ldots, N\}$, and the segment number is increased when going from the right-hand side to the left-hand side. The reactance of each segment is cancelled by its matching resonant capacitor. For a well-balance design purpose, that resonant capacitor could be separated into two identical capacitors located on each wire of the segment whose total equivalent value equals the matching resonant capacitor. Throughout this section, the compensating capacitors are denoted C_n and C'_n.

5.4.1 Unloaded Condition

In this part, we would like to focus on the unloaded condition as described in Fig. 5.4(a). Because the first segment is terminated in a short circuit, its input impedance before it is compensated by C_1 and C'_1 is

$$\begin{aligned} Z'_1(l) &= R'_1(l) + jX'_1(l) \\ &= Z_0 \tanh(\alpha l + j\beta l) \\ &= \frac{Z_0 \sinh 2\alpha l + jZ_0 \sin 2\beta l}{\cosh 2\alpha l + \cos 2\beta l} \end{aligned} \tag{5.15}$$

Because the segmentation length l is very short such that $\alpha l \ll 1$, $\sinh(2\alpha l) \approx 2\alpha l$ and $\cosh(2\alpha l) \approx 1$, $Z'_1(l)$ can be approximated as

$$Z'_1(l) = R'_1(l) + jX'_1(l) \approx \frac{Z_0 \alpha l}{\cos^2 \beta l} + jZ_0 \tan \beta l \tag{5.16}$$

The imaginary part $jX'_1(l) = jZ_0 \tan \beta l$ will be compensated for by two balanced capacitors C_1 and C'_1. As a result, the input impedance of the first segment after compensation is a purely real value

$$R'_1(l) = \mathrm{Re}\{Z'_1(l)\} \approx \frac{Z_0 \alpha l}{\cos^2 \beta l}. \tag{5.17}$$

This resistance is the terminating impedance for the second segment, thus the input impedance of the first two segments before compensation becomes

$$Z'_1(2l) = Z_0 \frac{R'_1(l) + Z_0 \tanh \gamma l}{Z_0 + R'_1(l) \tanh \gamma l} \tag{5.18}$$

As the segment length l is very short such that the phase change βl and the attenuation αl are very small, it is obvious that $R'_1(l)$ shown in Eq. (5.17) is very small compared to the characteristic impedance Z_0. As a result, the input impedance $Z'_1(2l)$ can be approximated as

$$\begin{aligned}
Z'_1(2l) &= R'_1(2l) + jX'_1(2l) \\
&= \frac{R'_1(l) + Z_0 \tanh \gamma l}{1 + \dfrac{R'_1(l)}{Z_0} \tanh \gamma l} \\
&= \frac{R'_1(l) + R'_1(l) + jX'_1(l)}{1 + \dfrac{R'_1(l)}{Z_0} \tanh \gamma l} \\
&\approx \frac{2R'_1(l) + jZ_0 \tan \beta l}{1 + \dfrac{R'_1(l)}{Z_0} \cdot \dfrac{R'_1(l)}{Z_0} + j\dfrac{R'_1(l)}{Z_0} \tan \beta l} \\
&\approx \frac{2R'_1(l) + jZ_0 \tan \beta l}{1 + j\dfrac{R'_1(l)}{Z_0} \tan \beta l} \\
&\approx [2R'_1(l) + jZ_0 \tan \beta l] \left[1 - j\frac{R'_1(l)}{Z_0} \tan \beta l\right] \\
&\approx \sum_{m=0}^{2-1} \left[\frac{1}{\cos^2 \beta l}\right]^m R'_1(l) + jZ_0 \tan \beta l
\end{aligned} \tag{5.19}$$

The imaginary part of $Z'_1(2l)$ is also $jZ_0 \tan \beta l$ which is equal to the reactance of the first segment $jX'_1(l)$. This means the resonant capacitors C_2 and C'_2 for the second segment are similar to the resonant capacitors C_1 and C'_1 for the first segment. The combined impedance of the first two segments after compensation is purely real

$$R'_1(2l) = \sum_{m=0}^{2-1} \left[\frac{1}{\cos^2 \beta l}\right]^m R'_1(l) \tag{5.20}$$

Similarly, it is obvious that the impedance of the first n segments before the resonant capacitor C'_n is

$$\begin{aligned}
Z'_1(nl) &= R'_1(nl) + jX'_1(nl) \\
&\approx \sum_{m=0}^{n-1} \left[\frac{1}{\cos^2 \beta l}\right]^m R'_1(l) + jZ_0 \tan \beta l
\end{aligned} \tag{5.21}$$

As shown in Eq. (5.21), the reactive component of $Z'_1(nl)$ is

$$X'_1(nl) \approx jZ_0 \tan \beta l \tag{5.22}$$

which is also equal to those of $Z'_1(l)$ and $Z'_1(2l)$. Thus, this component is cancelled by two balanced capacitors C_n and C'_n having the similar capacitances as the compensation capacitors of other segments. Consequently, the impedance of the first n segments after compensation has a purely real value

$$R'_1(nl) \approx \sum_{m=0}^{n-1} \left[\frac{1}{\cos^2 \beta l}\right]^m R'_1(l). \tag{5.23}$$

Eventually, the internal resistance of all the N segments after compensation, which is also the internal resistance of the transmitting coil in the proposed system is

$$\begin{aligned} R'_1 \triangleq R'_1(Nl) &\approx \frac{1 - \left[\frac{1}{\cos^2 \beta l}\right]^N}{1 - \frac{1}{\cos^2 \beta l}} R'_1(l) \\ &\approx \frac{1 - \left[\frac{1}{\cos^2 \beta L/N}\right]^N}{1 - \frac{1}{\cos^2 \beta L/N}} \frac{Z_0 \alpha L/N}{\cos^2 \beta L/N} \end{aligned} \tag{5.24}$$

The value of R'_1 in Eq. (5.24) for the special case $N = 1$ is $Z_0 \alpha L / \cos^2 \beta L$, which is similar to the internal resistance R_1 of the non-segmented PLF in Eq. (5.3). Because Eq. (5.24) is not a monotonically increasing function of N, it is hard to say that R'_1 decreases immediately from the initial value R_1 when we increase the number of segments N to 2 or 3. However, when N is sufficiently large such that the value of $\cos^2 \beta L/N$ approaches 1, the value of R'_1 reduces and will approach $Z_0 \alpha L$. In such a case, the segmented PLF behaves like a lumped-element and R'_1 reflects losses in the loaded condition. A reduction of R'_1 therefore pays contribution to efficiency improvement for the segmented PLF. The significance of reducing the feeder resistance is therefore more obvious to this system than to the conventional non-segmented one.

5.4.2 Loaded Condition

Now, let us consider the segmented feeder in loaded condition illustrated in Fig. 5.4(b). Without loss of generality, let us assume that the feeder couples with the receiver coil at the n-th segment. In this case, the input impedances of the first, the second, ... and the $(n-1)$-th segments remain unchanged from their conditions in the unloaded case in Sect. 5.4.1. However, the input impedance of the n-th segment changes from Eq. (5.23) because the load R_L reflects an impedance $\omega^2 M^2/(R_2+R_L)$ onto this segment via the mutual inductance M. As a result, the impedance of the first n-th segments in loaded condition becomes

$$\begin{aligned} R'_{in}(nl) &= R'_1(nl) + \frac{\omega^2 M^2}{R_2 + R_L} \\ &\approx \sum_{m=0}^{n-1} \left[\frac{1}{\cos^2 \beta l}\right]^m R'_1(l) + \frac{\omega^2 M^2}{R_2 + R_L} \end{aligned} \tag{5.25}$$

In Eq. (5.25), the first term represents the total internal resistances of the first n segments and the second term represents the reflected impedance of the load onto the feeder.

The $(n+1)$-th segment is terminated in $R'_{in}(nl)$. Therefore, the impedance of the first $(n+1)$ segments including the load can be expressed as follows.

$$\begin{aligned} Z'_{in}((n+1)l) &= R'_{in}((n+1)l) + jX'_{in}((n+1)l) \\ &= \frac{R'_{in}(nl) + Z_0 \tanh \gamma l}{1 + \dfrac{R'_{in}(nl)}{Z_0} \tanh \gamma l} \end{aligned} \tag{5.26}$$

As $R'_{in}(nl) \ll Z_0$ and $Z_0 \tanh \gamma l = R'_1(l) + jZ_0 \tan \beta l$, we can approximate $Z'_{in}((n+1)l)$ as follows.

$$\begin{aligned} Z'_{in}((n+1)l) &\approx [R'_1(nl) + R'_1(l) + jZ_0 \tan \beta l] \\ &\quad \times \left[1 - j\frac{R'_1(l)}{Z_0} \tan \beta l\right] \\ &\approx \sum_{m=0}^{n} \left[\frac{1}{\cos^2 \beta l}\right]^m R'_1(l) \\ &\quad + \frac{1}{\cos^2 \beta l} \frac{\omega^2 M^2}{R_2 + R_L} + jZ_0 \tan \beta l \end{aligned} \tag{5.27}$$

In Eq. (5.27), the imaginary part will be cancelled by the compensation capacitors

C_{n+1} and C'_{n+1}, resulting in a pure resistance

$$R'_{\text{in}}((n+1)l) \approx \sum_{m=0}^{n} \left[\frac{1}{\cos^2 \beta l}\right]^m R'_1(l) + \frac{1}{\cos^2 \beta l} \frac{\omega^2 M^2}{R_2 + R_L} \tag{5.28}$$

Eventually, input impedance of the whole segmented feeder in the loaded condition is

$$\begin{aligned} R'_{\text{in}} &\triangleq R'_{\text{in}}(Nl) \\ &\approx \sum_{m=0}^{N-1} \left[\frac{1}{\cos^2 \beta l}\right]^m R'_1(l) + \left[\frac{1}{\cos^2 \beta l}\right]^{N-n} \frac{\omega^2 M^2}{R_2 + R_L} \\ &\approx \frac{1 - \left[\dfrac{1}{\cos^2 \beta l}\right]^N}{1 - \dfrac{1}{\cos^2 \beta l}} R'_1(l) + \left[\frac{1}{\cos^2 \beta l}\right]^{N-n} \frac{\omega^2 M^2}{R_2 + R_L} \\ &\approx R'_1 + \left[\frac{1}{\cos^2 \beta l}\right]^{N-n} \frac{\omega^2 M^2}{R_2 + R_L} \end{aligned} \tag{5.29}$$

From Eq. (5.29), the kQ-product of this system can be expressed as

$$\chi'(nl) = \frac{\omega^2 M^2}{R'_1 R_2} \cdot \left[\frac{1}{\cos^2 \beta l}\right]^{N-n} \tag{5.30}$$

Thus, the maximum achievable efficiency of the segmented PLF system is given by

$$\eta'_{\max}(nl) = 1 - \frac{2}{1 + \sqrt{1 + \dfrac{\omega^2 M^2}{R'_1 R_2} \cdot \left[\dfrac{1}{\cos^2 \beta L/N}\right]^{N-n}}} \tag{5.31}$$

It is obvious looking at Eq. (5.31) that the maximum achievable efficiency does not vary based on the receiver's position. So, the segmentation of the PLF makes it robust against the position of the receiver. However, it also shows that the efficiency is not a constant. It may slightly vary with n when the receiver moves from one segment to the other. To be specific, the receiver moves to the left-hand side (closer to the source), the maximum efficiency decreases. The efficiency has the highest value when the receiver is at the first segment and has the lowest value when the receiver at the N-th segment. The lowest value of efficiency is an increasing function of the term $\omega^2 M^2/(R'_1 R_2)$. This implies that by sufficiently

Table 5.2: Added capacitors and input reactance for 5-segment PLF

Segment number n	Length nl	Capacitor (pF)		Reactance (Ω)
		C_n	C'_n	$X'_1(nl)$
1	1	no capacitors		363.4
		30	**29**	**0.8**
2	2	no capacitors		340.9
		35	**35**	**-0.8**
3	3	no capacitors		364.9
		35	**31**	**1**
4	4	no capacitors		367.5
		34	**33**	**-0.8**
5	5	no capacitors		356.8
		36	**36**	**0.5**

shortening the feeder length, it is able to reduce the resistance R'_1 and improve the efficiency.

Also in Eq. (5.31) , the magnitude of the term $\cos(\beta L/N)$ decides how drastic the efficiency variation is. When this value is far from 1, the efficiency variation is dynamic, but when this value is close to 1, the efficiency variation is quite slow. Therefore, we can stabilize the system efficiency by using the segmented PLF with a sufficiently shortened segment length l.

5.5 Experimental results

5.5.1 Resonance effect

Figure 5.5 shows a sample of the S_{11} and S_{22} parameters for the 10-segmented PLF when the receiver is at the position 75 cm from the end of the line. We can clearly see that the PLF and the coil are resonating around the frequency of 27.12 MHz. The coupling seems to be weak but the high frequency compensated with a high Q making the system achieving the maximum efficiency for that configuration.

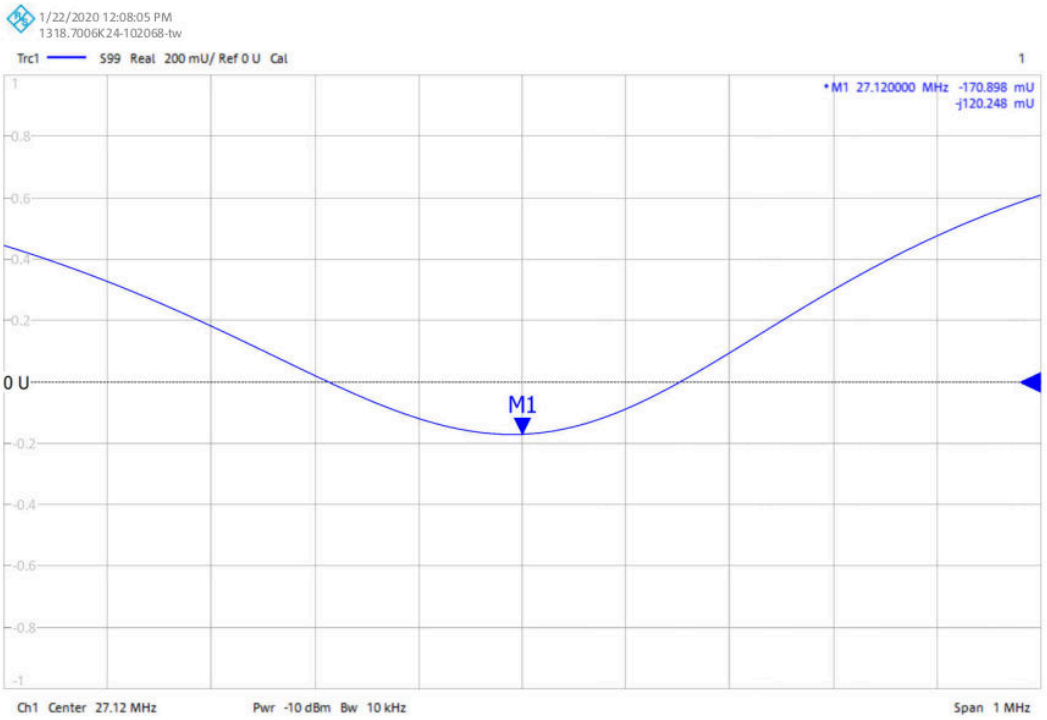

(a) S_{11}

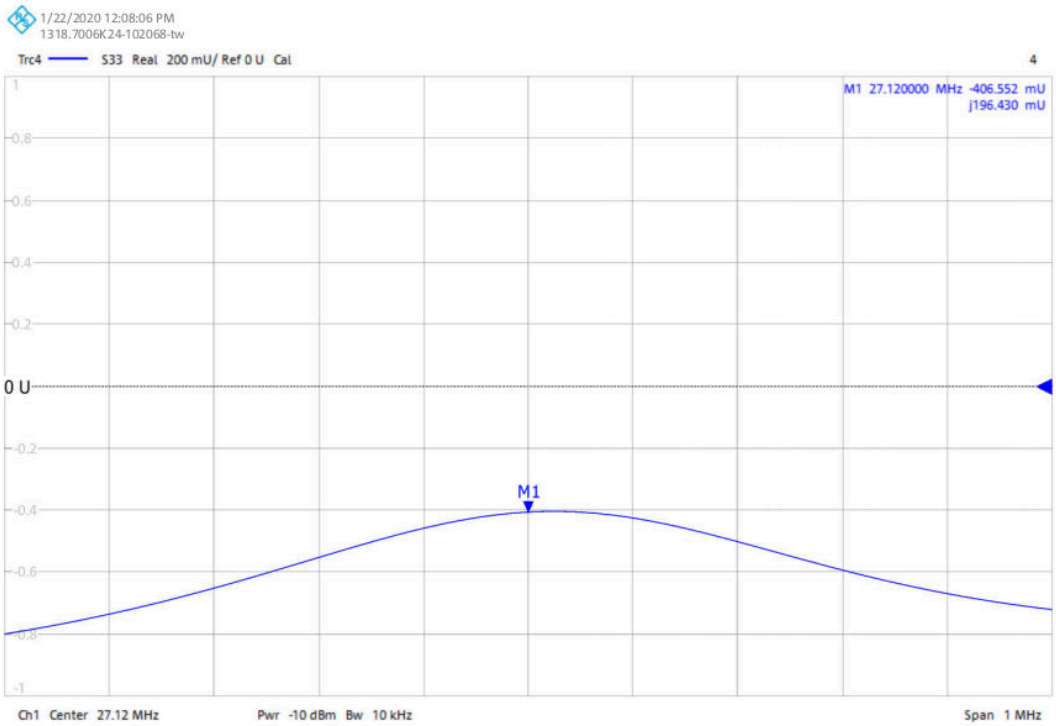

(b) S_{22}

Figure 5.5: Scattering parameters plot for the 10-segmented PLF

Table 5.3: Added capacitors and input reactance for 10-segment PLF

Segment number n	Length nl	Capacitor (pF)		Reactance (Ω)
		C_n	C'_n	$X'_1(nl)$
1	0.5	no capacitors		107.3
		64	**64**	**1**
2	1	no capacitors		152.5
		76	**76**	**-0.7**
3	1.5	no capacitors		150.2
		79	**82**	**-0.5**
4	2	no capacitors		160.2
		75	**76**	**0.1**
5	2.5	no capacitors		153.2
		80	**77**	**-0.3**
6	3	no capacitors		158.9
		77	**77**	**0.4**
7	3.5	no capacitors		160
		78	**76**	**-0.4**
8	4	no capacitors		159.1
		79	**78**	**0**
9	4.5	no capacitors		157.9
		80	**77**	**-0.1**
10	5	no capacitors		164.9
		76	**76**	**-0.9**

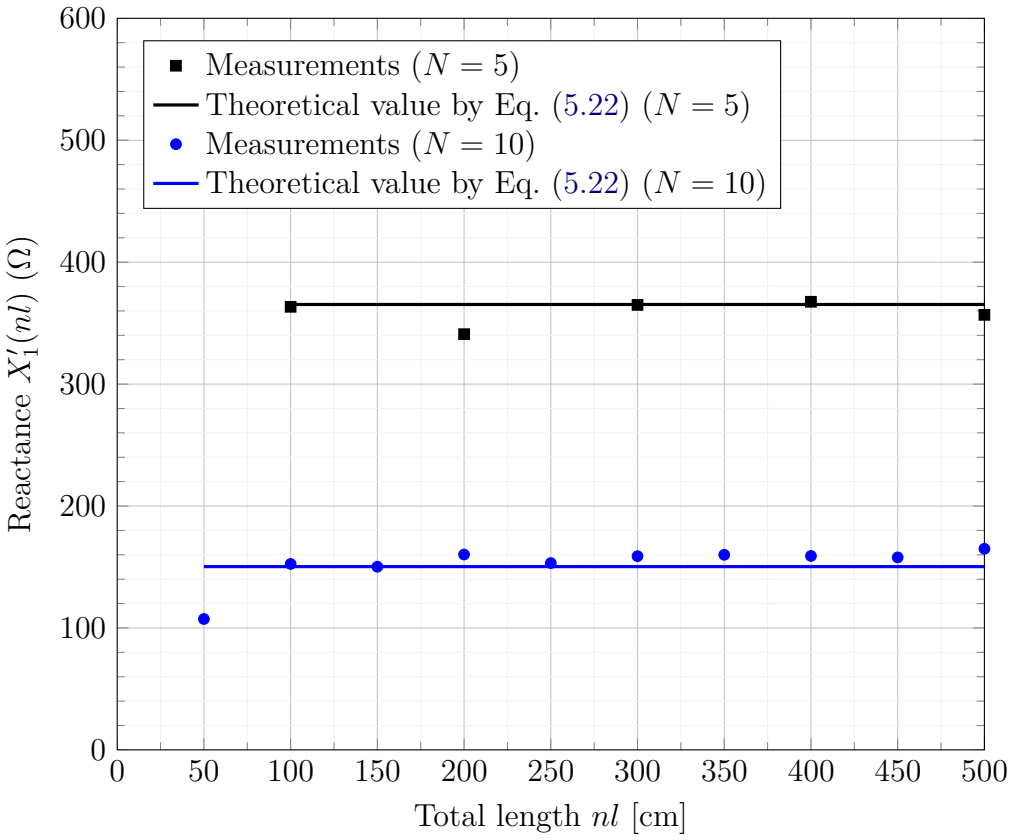

Figure 5.6: Reactance of segmented PLF as a function of feeder length.

5.5.2 Loss reduction effect

This section presents the experiments results of the segmented PLF in the unloaded condition to evaluate the impact of the segmentation on the feeder losses. In order to make that evaluation, we built two different versions of the segmented PLF. The first version has the number of segments $N = 5$ with each having the length of $l_1 = 1$ m; The second implementation on the other hand has $N = 10$ segments of identical length $l_2 = 0.5$ m. This means both the two segmented versions have the same total length $L = 5$ m as the non-segmented PLF in Sect. 5.2.1.

Experimental setup of the 5-segment version is shown in Tab. 5.2 and that of the 10-segment version is described in Tab. 5.3. Tab. 5.2 and Tab. 5.3 summarize the parameters of the resonant capacitors as well as the impedance of line at each segment before and after inserting the resonant capacitors. We can notice that the capacitors have been chosen to properly cancel the reactive component. The

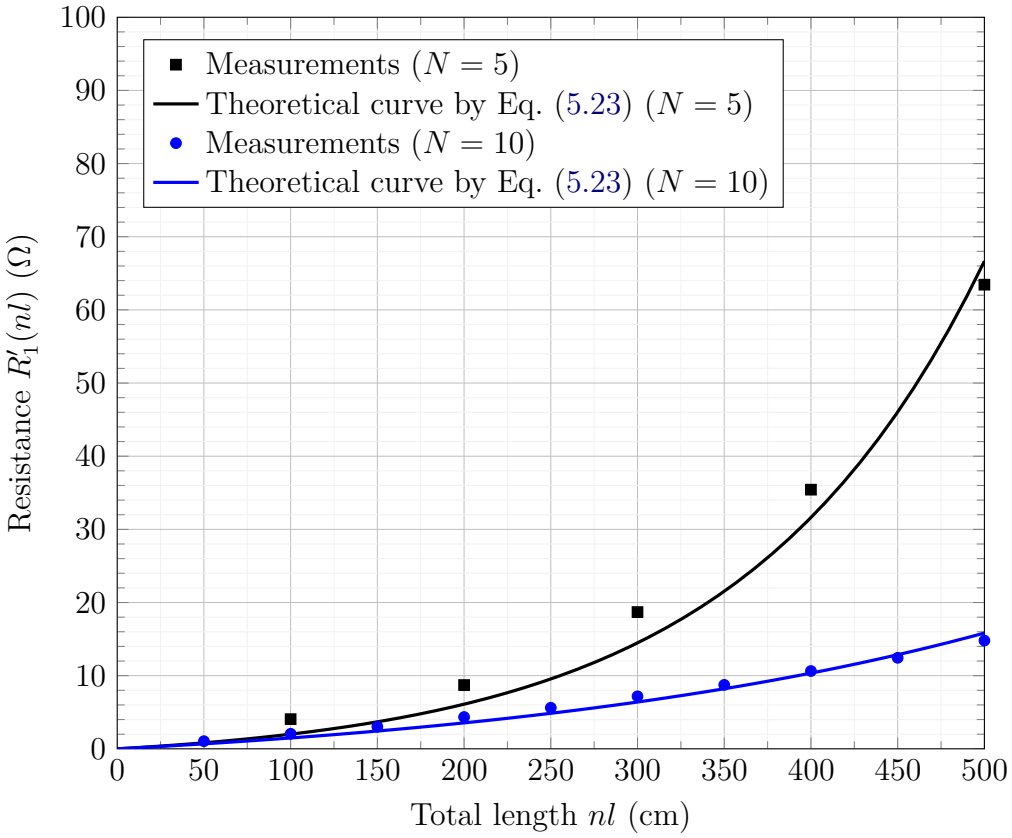

Figure 5.7: Resistance of segmented PLF as a function of feeder length.

other parameters related to the feeder configuration are the same as of the non-segmented PLF. As for the values of resonant capacitors, there is a good match between the values in Tab. 5.2 and Tab. 5.3 and the theoretical analysis in Sect. 3. In Tab. 5.2, the resonant capacitors have similar values for all 5 segments. In Tab. 5.3, except for the first segment, the remaining 9 segments have similar resonant capacitors.

Figure 5.6 confirms the observation in Eq. (5.22) that $X_1'(nl) = Z_0 \tan \beta l$ for all $n = 1, 2, \ldots N$. The vertical axis of the figure shows the reactance $X_1'(nl)$ for the 5-segment version and the 10-segment version of the PLF. The measurements are shown by the dots; and the theoretical values calculated by Eq. (5.21) are indicated by the horizontal lines. For the 5-segment version, the measurements are close to the theoretical value of 365.3 Ω. Similarly, for the 10-segment version, the measurements are close to the theoretical value of 150.3 Ω.

Figure 5.7 verifies the theoretical formula for internal resistance of the segmented PLF shown in Eq. (5.23). The measurements for the internal resistance are demonstrated by the dots and the theoretical curves by Eq. (5.23) are expressed by the lines. As shown in the figure, for each version of the feeder, the measurements fit well to the associated theoretical curve; and the internal resistance increases with the total length $L = nl$. More importantly, the 10-segment version has a smaller resistance than that of the 5-segment version. The resistance of the 10-segment version is only 14.8 Ω, which is significantly reduced compared to 63.3 Ω resistance of the 5-segment version. This implies that the losses can be significantly reduced by properly shortening the segment length.

5.5.3 Efficiency improvement and stabilization effects

Using the same receiver coils as in Sect. 5.2.1, we measure the maximum achievable efficiency for the two versions of the segmented PLF in Sect. 5.5.2. The air gap between the receiver coil and the feeder is kept unchanged at 2 mm. Following the same process in Sect. 5.2.1, for each position of the receiver coil along the feeder, we measure the Z-parameters and substitute them into Eq. (5.14) to calculate the maximum efficiency. The results of this measurement is shown by the triangle dots and circle dots in Fig. 5.8. This figure also plots theoretical curves for the maximum efficiency by using the measured values of parameters M, β, R_1' and R_2 and by following Eq. (5.31). In this figure, the measurements and theoretical curve for efficiency of the single-segment PLF system are also demonstrated for comparison.

As shown in Fig. 5.8 for the 5-segment PLF, the measurements agree well with the theoretical curve. Also, it is obvious that the efficiency of the 5-segment PLF does not fluctuates drastically following a standing wave pattern as in the

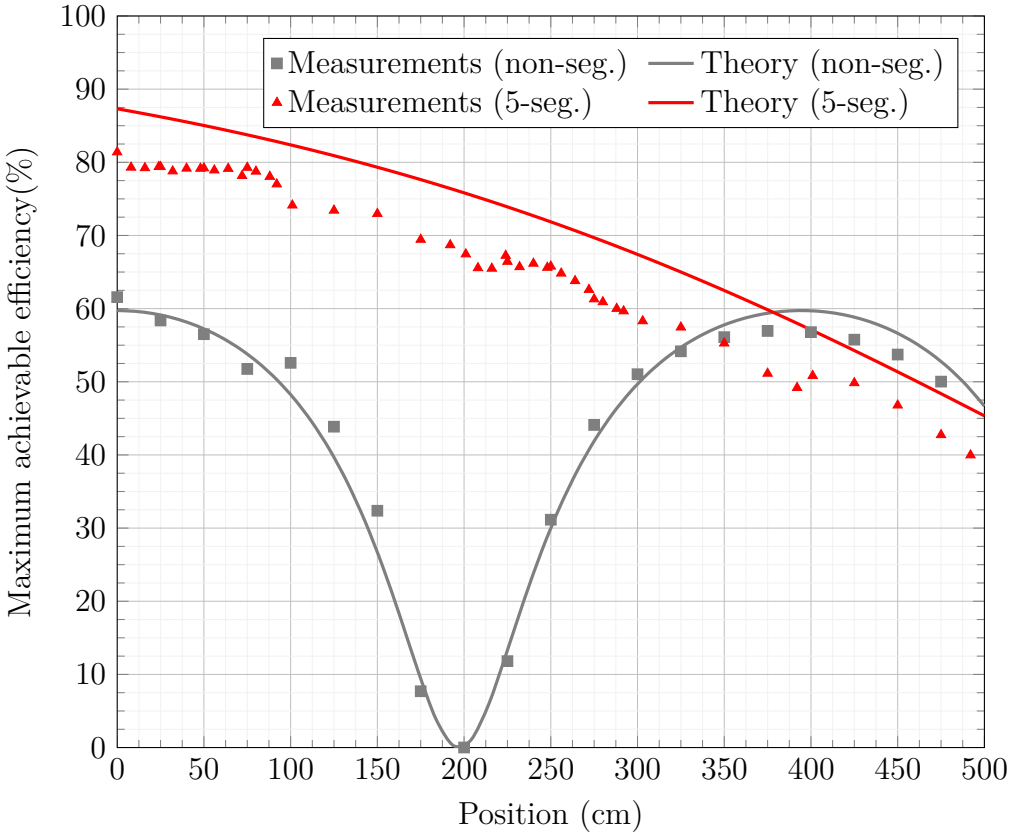

Figure 5.8: Efficiency comparison between 5-segment PLF and non-segmented PLF.

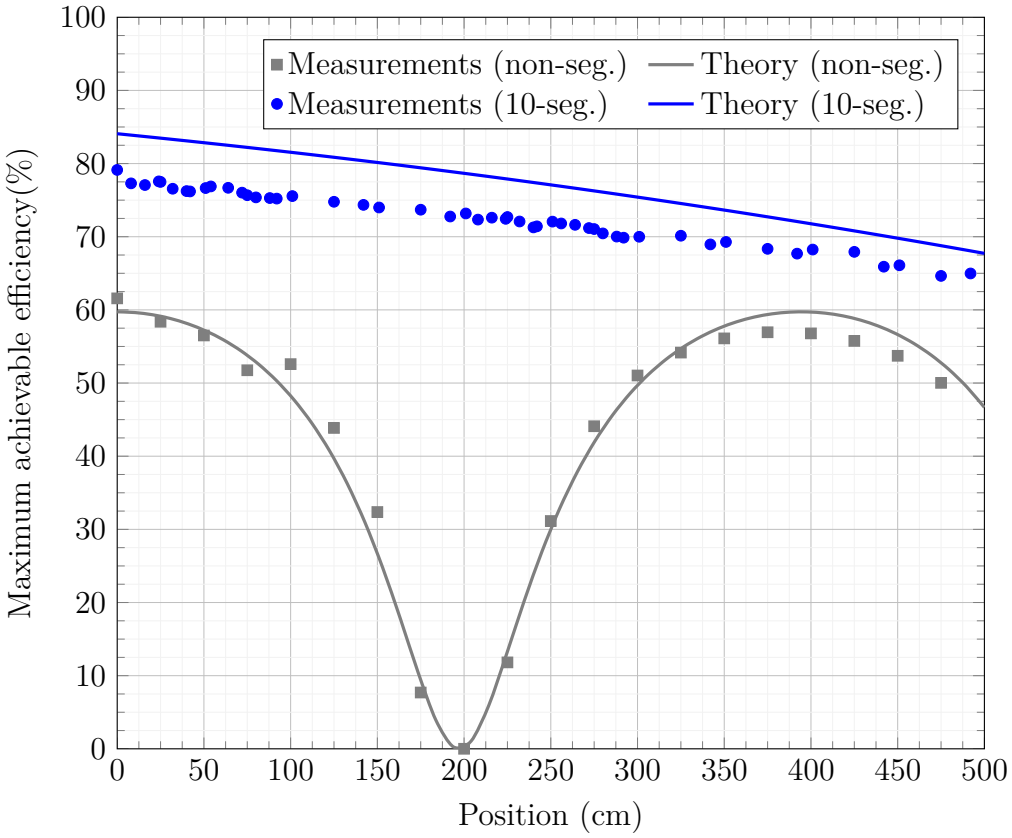

Figure 5.9: Efficiency comparison between 10-segment and non-segmented PLF.

non-segmented one. Even that the 5-segment version exhibits a more stable performance, its efficiency gradually decreases from about 80% to around 40% as the receiver moves from the terminating end toward the source. This characteristic of the segmented PLF agrees with the theoretical analysis in Chap. 5. The efficiency of the 5-segment PLF averaged over all the receiver positions is about 60%. Meanwhile, the non-segmented PLF demonstrates a fluctuation in efficiency between the highest value of around 60% and the lowest value of 0%, meaning its average efficiency over all receiver positions is around 30%. This result confirm that the 5-segment version has a more stable and higher efficiency than the non-segmented one.

Figure 5.9 shows that the efficiency of the 10-segment version decreases from the highest value of around 80% to the lowest value of about 60%; and the average efficiency over all receiver positions is about 70%. Obviously, the 10-segment PLF exhibits an even more stable and higher efficiency performance compared to the 5-segment version. This result verifies that the efficiency can be improved and stabilized by properly shortening the segment length of the PLF.

5.6 Summary

The investigation of the segmented PLF with two different segmentation schemes demonstrated that the maximum achievable efficiency of the PLF could be significantly increased. In fact, it showed that reducing the length of each segment helps has a beneficial impact on the reduction of the internal resistance of the whole segmented PLF thus reducing the PLF losses and improving its power efficiency. That segments size reduction has the effect of stabilizing the efficiency as well. The experiments showed that further reducing the segment length reduces the slope of the tangent near to zero making it almost constant all over the PLF length regardless of the receiver position. Also, the fact that all the compensation capacitors have the same value considerably improves the design and reduces the maintenance burden of the PLF which is a must for it to be practical.
It can therefore be industrialized, with simple steps as:

1. Construct the first segment from the end of the line (short-circuit)
2. Measure its impedance (mainly self inductance)
3. Compensate with a set of corresponding capacitors to make it resonant
4. Add the same length and resonance capacitors for all subsequent segments until the desired PLF size is built.

6 Conclusions and future research

6.1 Conclusions

This research focused on methods to mitigate the intrinsic standing wave appearing on the parallel line feeder as it acts as a transmission line. First a combination of multiple PLF using the MIMO techniques for diversity and multiplexing effect was employed. It helped to mitigate the standing wave issue with higher stability and output power but was suffering from other issues related to the dielectric losses. Therefore, the investigation of a new scheme of the PLF as a multiple segments concatenated together was performed. The early simulations and experiments demonstrated that this approach could display a more uniform magnetic field while resolving the aforementioned issues. Lastly, in order to make the segmented PLF practical, the need to evaluate it upper-bound performance arises. The last steps of this dissertation attempted to derive the maximum achievable efficiency for a considerably long parallel line feeder (5 m) in order to analyze its performance for real applications. For that purpose, the PLF was modeled as a lossy transmission line. In the single segment PLF, the theoretical analysis inferred that the efficiency still exhibits the standing wave pattern according to the position x of the receiver. The experiments conducted at the operating frequency of a 27.12 MHz confirms that theory by showing the power is dropping from a peak around 60% to 0% and increased again to the peak at position 0 cm, 200 cm and 400 cm respectively and the trend is repeating. With that drastic fluctuations, the PLF cannot be a suitable candidate for practical applications. Therefore, the segmented PLF has been investigated. Its maximum achievable efficiency formulation suggests that it is not affected by the position x of the receiver and is more stable all over the length of the PLF. Experiments with two different segmentation configuration of the PLF have been performed. One with the 5 segments with each of length 1m and the other with 10 segments where each segment is 0.5m long. The results of these experiments show significant impact of the segmentation over the non-segmented PLF with improved efficiency and stability. This has been possible thanks to the loss reduction and the uniform magnetic field introduced by the short length of the segments. In-

deed, the 5-segment PLF has a reactance $X_1'(nl) \approx 365.3\ \Omega$ for all $n = 1, 2, \ldots N$ and its efficiency gradually fluctuates from about 80% to around 40% as the receivers travels from the end of the line to the source. The impacts are more significant with the 10-segment scheme where the reactance of $X_1'(nl) \approx 150.3\ \Omega$ and the efficiency fluctuates only from 80% to 60% making an average of 70% all over the PLF length. This results shows that further reducing the segment length improves the PLF performance. So, with that amelioration through the segmentation, the PLF can be considered as a practical solution for IPT.

6.2 Future research

Since the overall performance of a IPT system is mostly governed by its transmission efficiency, the current investigations on the maximum achievable RF-to-RF efficiency formulation did not need to invest into the receiver design as a priority. Nevertheless, they demonstrated that the segmented PLF is a practical system which was supported by the experiments. However, for the PLF to be adopted as a consumer device, the DC-to-DC performance needs to be investigated. As previously mentioned, the current investigations did not take into account the circuit design including impedance matching and filtering for the PLF or the receiver which is an essential step for the end-to-end (DC-to-DC) system design implementation.
Also, up to now, the segmented PLF performance evaluation focused on a single receiver for the analysis. So, it will be interesting to investigate the performance in case of multiple receivers in order to leverage the extensibility of the PLF.

Acknowledgments

First and foremost, I would like to express my sincere gratitude to my supervisor Professor Minoru Okada for his support and guidance during my research.
Besides, I would like to thank all the professors in the Network Systems laboratory for the help during the research. My deepest thanks goes to Professor Duong Quang Thang for his dedication to the accomplishment of this work with whom I spent tremendous time discussing and without whom this would have not been possible.
Moreover, I would like to reiterate my thanks to my professors but also to all the staff of the Nara Institute of Science and Technology for their warm assistance during my personal life struggles.

Thank you to Associate Professor Duy Ngo of School of Electrical Engineering and Computing at Newcastle University in Australia and his team members, for giving me the chance to have an enriching experience during the internship in his laboratory.

My gratitude to the Japanese Ministry of Education, Culture, Sports, Science and Technology (MEXT) which granted me a scholarship and financially supported my Master Degree and Doctoral Course in Japan and to JSPS KAKENHI for supporting this work with the Grant Number 19K04376.

Most of all, to my parents for their encouragement with special consideration to my big brother and my father who passed away during my PhD term, I would like to say huge thanks. You have always been there for me and I will always love you. Rest in Peace !

References

[1] Wikipedia contributors, "Wardenclyffe tower — Wikipedia, the free encyclopedia," 2022. [Online; accessed 6-December-2022].

[2] H. W. Secor, *Tesla Apparatus and Experiments—How to Build Both Large and Small Tesla and Oudin Coils and How to Carry On Spectacular Experiments With Them.* Associate Member American Institute of Electrical Engineers, Nov. 1921.

[3] R. R. Harrison, "Designing efficient inductive power links for implantable devices," in *2007 IEEE International Symposium on Circuits and Systems*, pp. 2080–2083, 2007.

[4] S. Atluri and M. Ghovanloo, "Design of a wideband power-efficient inductive wireless link for implantable biomedical devices using multiple carriers," in *Conference Proceedings. 2nd International IEEE EMBS Conference on Neural Engineering, 2005.*, pp. 533–537, 2005.

[5] M. Sawan, Y. Hu, and J. Coulombe, "Wireless smart implants dedicated to multichannel monitoring and microstimulation," *IEEE Circuits and Systems Magazine*, vol. 5, no. 1, pp. 21–39, 2005.

[6] C. Sauer, M. Stanacevic, G. Cauwenberghs, and N. Thakor, "Power harvesting and telemetry in cmos for implanted devices," *IEEE Transactions on Circuits and Systems I: Regular Papers*, vol. 52, no. 12, pp. 2605–2613, 2005.

[7] S. Jeong, Y. J. Jang, and D. Kum, "Economic analysis of the dynamic charging electric vehicle," *IEEE Transactions on Power Electronics*, vol. 30, pp. 6368–6377, nov 2015.

[8] S. Jeong, Y. J. Jang, D. Kum, and M. S. Lee, "Charging automation for electric vehicles: Is a smaller battery good for the wireless charging electric vehicles?," *IEEE Transactions on Automation Science and Engineering*, vol. 16, pp. 486–497, jan 2019.

[9] D. M. Nguyen, M. A. Kishk, and M.-S. Alouini, "Modeling and analysis of dynamic charging for EVs: A stochastic geometry approach," *IEEE Open Journal of Vehicular Technology*, vol. 2, pp. 17–44, 2021.

[10] A. M. Research, "Wireless power transmission market."

[11] T. Higashino, M. Ziji, M. Okada, Y. Tatsuta, Y. Goto, Y. Tsuruda, and R. Tanaka, "A new configuration of magnetic coupled power transfer using parallel line feeder," in *2013 IEEE Wireless Power Transfer (WPT)*, IEEE, 2013.

[12] Z. Zhang, H. Pang, A. Georgiadis, and C. Cecati, "Wireless power transfer—an overview," *IEEE Transactions on Industrial Electronics*, vol. 66, pp. 1044–1058, feb 2019.

[13] L. Xie, Y. Shi, Y. T. Hou, and A. Lou, "Wireless power transfer and applications to sensor networks," *IEEE Wireless Communications*, vol. 20, pp. 140–145, aug 2013.

[14] N. Shinohara, "Trends in wireless power transfer: WPT technology for energy harvesting, mllimeter-wave/THz rectennas, MIMO-WPT, and advances in near-field WPT applications," *IEEE Microwave Magazine*, vol. 22, pp. 46–59, jan 2021.

[15] B. M. Adarsha, S. Prakash, V. G. Naik, and K. V. Reddy, "Wireless power transfer for wireless sensor networks using hybrid algorithm," in *2017 International Conference on Computing Methodologies and Communication (ICCMC)*, IEEE, jul 2017.

[16] S. He, J. Chen, F. Jiang, D. K. Yau, G. Xing, and Y. Sun, "Energy provisioning in wireless rechargeable sensor networks," *IEEE Transactions on Mobile Computing*, vol. 12, pp. 1931–1942, oct 2013.

[17] Y. Peng, Z. Li, W. Zhang, and D. Qiao, "Prolonging sensor network lifetime through wireless charging," in *2010 31st IEEE Real-Time Systems Symposium*, IEEE, nov 2010.

[18] T. Ajmal, D. Jazani, and B. Allen, "Design of a compact RF energy harvester for wireless sensor networks," in *IET Conference on Wireless Sensor Systems (WSS 2012)*, IET, 2012.

[19] W. Brown, "The history of power transmission by radio waves," *IEEE Transactions on Microwave Theory and Techniques*, vol. 32, pp. 1230–1242, sep 1984.

[20] B. Strassner and K. Chang, "Microwave power transmission: Historical milestones and system components," *Proceedings of the IEEE*, vol. 101, pp. 1379–1396, jun 2013.

[21] PowerCast, "Powercast corp.."

[22] A. Sample, D. Yeager, P. Powledge, A. Mamishev, and J. Smith, "Design of an RFID-based battery-free programmable sensing platform," *IEEE Transactions on Instrumentation and Measurement*, vol. 57, no. 11, pp. 2608–2615, 2008.

[23] M. Fantuzzi, M. D. Prete, D. Masotti, and A. Costanzo, "Quasi-isotropic RF energy harvester for autonomous long distance IoT operations," in *2017 IEEE MTT-S International Microwave Symposium (IMS)*, IEEE, 2017.

[24] Z. Popovic, "Far-field wireless power delivery and power management for low-power sensors," in *2013 IEEE Wireless Power Transfer (WPT)*, IEEE, may 2013.

[25] G. A. Covic and J. T. Boys, "Inductive power transfer," *Proceedings of the IEEE*, vol. 101, pp. 1276–1289, jun 2013.

[26] A. Kurs, A. Karalis, R. Moffatt, J. Joannopoulos, P. Fisher, and M. Soljacic, "Wireless power transfer via strongly coupled magnetic resonances," *Science*, vol. 317, pp. 83–86, jul 2007.

[27] W. Y. Lee, J. Huh, S. Y. Choi, X. V. Thai, J. H. Kim, E. A. Al-Ammar, M. A. El-Kady, and C. T. Rim, "Finite-width magnetic mirror models of mono and dual coils for wireless electric vehicles," *IEEE Transactions on Power Electronics*, vol. 28, pp. 1413–1428, mar 2013.

[28] U.-M. Jow and M. Ghovanloo, "Geometrical design of a scalable overlapping planar spiral coil array to generate a homogeneous magnetic field," *IEEE Transactions on Magnetics*, vol. 49, pp. 2933–2945, jun 2013.

[29] Q. Zhu, L. Wang, Y. Guo, C. Liao, and F. Li, "Applying lcc compensation network to dynamic wireless ev charging system," *IEEE Transactions on Industrial Electronics*, vol. 63, no. 10, pp. 6557–6567, 2016.

[30] J. Li, F. Yin, L. Wang, B. Cui, and D. Yang, "Electromagnetic induction position sensor applied to anti-misalignment wireless charging for UAVs," *IEEE Sensors Journal*, vol. 20, pp. 515–524, jan 2020.

[31] X. Dang, P. Jayathurathnage, S. A. Tretyakov, and C. R. Simovski, "Self-tuning multi-transmitter wireless power transfer to freely positioned receivers," *IEEE Access*, vol. 8, pp. 119940–119950, 2020.

[32] V. K. Srivastava, A. Sharma, and A. Bharadwaj, "A planar distributed multicoil antenna to generate 3-d ellipsoidally polarized h-field for angular misalignment tolerant WPT system," *IEEE Transactions on Antennas and Propagation*, vol. 70, pp. 2969–2978, apr 2022.

[33] M. Zargham and P. G. Gulak, "Maximum achievable efficiency in near-field coupled power-transfer systems," *IEEE Transactions on Biomedical Circuits and Systems*, vol. 6, pp. 228–245, jun 2012.

[34] T. Ohira, "Maximum available efficiency formulation based on a black-box model of linear two-port power transfer systems," *IEICE Electronics Express*, vol. 11, no. 13, pp. 20140448–20140448, 2014.

[35] T. Ohira, "Extended k-q product formulas for capacitive- and inductive-coupling wireless power transfer schemes," *IEICE Electronics Express*, vol. 11, no. 9, pp. 20140147–20140147, 2014.

[36] T. OHIRA, "Power transfer theory on linear passive two-port systems," *IEICE Transactions on Electronics*, vol. E101.C, no. 10, pp. 719–726, 2018.

[37] WirelessPowerConsortium, "Qi standard."

[38] Q.-T. Duong and M. Okada, "Inductive power transmission using multiple concatenated parallel-line-feeder segments," in *2016 IEEE Wireless Power Transfer Conference (WPTC)*, IEEE, 2016.

[39] W.-F. Brou, Q.-T. Duong, and M. Okada, "Experimental evaluation of inductive power transfer system using multiple concatenated parallel-line-feeder segments," in *2016 International Symposium on Antennas and Propagation (ISAP)*, pp. 510–511, 2016.

[40] D. M. Pozar, *Microwave engineering*. Wiley, 2011.

[41] K. Kaiser, *Transmission Lines, Matching, and Crosstalk*. Taylor & Francis, 2005.

[42] T. Macnamara, *Introduction to Antenna Placement and Installation*. Aerospace Series, Wiley, 2010.

[43] N. Tesla, "The transmission of electric energy without wires," *Electrical World and Engineer*, Mar. 1904.

[44] N. Tesla, *Experiments with Alternate Currents of High Potential and High Frequency.* 1904.

[45] W. C. Brown, "Experimental airborne microwave supported platform," 1965.

[46] W. C. Brown, "Experiments involving a microwave beam to power and position a helicopter," *IEEE Transactions on Aerospace and Electronic Systems*, vol. AES-5, no. 5, pp. 692–702, 1969.

[47] A. Celeste, P. Jeanty, and G. Pignolet, "Case study in reunion island," *Acta Astronautica - ACTA ASTRONAUT*, vol. 54, pp. 253–258, 02 2004.

[48] Y.-K. Chen, "Challenges and opportunities of internet of things," in *17th Asia and South Pacific Design Automation Conference*, pp. 383–388, 2012.

[49] A. Takacs, H. Aubert, L. Despoisse, and S. Fredon, "Microwave energy harvesting for satellite applications," *Electronics Letters*, vol. 49, pp. 722–724, may 2013.

[50] A. Takacs, H. Aubert, L. Despoisse, and S. Fredon, "Design and implementation of a rectenna for satellite application," in *2013 IEEE Wireless Power Transfer (WPT)*, pp. 183–186, 2013.

[51] A. N. Parks, A. P. Sample, Y. Zhao, and J. R. Smith, "A wireless sensing platform utilizing ambient rf energy," in *2013 IEEE Topical Conference on Biomedical Wireless Technologies, Networks, and Sensing Systems*, pp. 154–156, 2013.

[52] F. Alneyadi, M. Alkaabi, S. Alketbi, S. Hajraf, and R. Ramzan, "2.4ghz wlan rf energy harvester for passive indoor sensor nodes," in *2014 IEEE International Conference on Semiconductor Electronics (ICSE2014)*, pp. 471–474, 2014.

[53] E. A. Kadir, A. P. Hu, M. Biglari-Abhari, and K. C. Aw, "Indoor wifi energy harvester with multiple antenna for low-power wireless applications," in *2014 IEEE 23rd International Symposium on Industrial Electronics (ISIE)*, pp. 526–530, 2014.

[54] A. Eid, J. G. D. Hester, and M. M. Tentzeris, "5g as a wireless power grid," *Scientific Reports*, vol. 11, jan 2021.

[55] H. Fnato, Y. Chiku, and K. Harakawa, "Wireless power distribution with capacitive coupling excited by switched mode active negative capacitor," in *2010 International Conference on Electrical Machines and Systems*, pp. 117–122, 2010.

[56] M. Kline, I. Izyumin, B. Boser, and S. Sanders, "Capacitive power transfer for contactless charging," in *2011 Twenty-Sixth Annual IEEE Applied Power Electronics Conference and Exposition (APEC)*, pp. 1398–1404, 2011.

[57] S. Y. Hui, "Planar wireless charging technology for portable electronic products and qi," *Proceedings of the IEEE*, vol. 101, no. 6, pp. 1290–1301, 2013.

[58] S. L. Ho, J. Wang, W. N. Fu, and M. Sun, "A comparative study between novel witricity and traditional inductive magnetic coupling in wireless charging," *IEEE Transactions on Magnetics*, vol. 47, no. 5, pp. 1522–1525, 2011.

[59] "Wireless power demonstrated." http://thefutureofthings.com/5569-wireless-power-demonstrated/. (Accessed on 01/15/2017).

[60] M. Stratmann and P. Trawinski, "Rechargeable toothbrushes with charging stations," U.S. Patent No.6,798,169, Issued - 09/28/2004.

[61] O. Mourad, P. Le Thuc, R. Staraj, and P. Iliev, "System modeling of the rfid contactless inductive coupling using 13.56 mhz loop antennas," in *The 8th European Conference on Antennas and Propagation (EuCAP 2014)*, pp. 2034–2038, 2014.

[62] H. Jiang, J. Zhang, D. Lan, K. K. Chao, S. Liou, H. Shahnasser, R. Fechter, S. Hirose, M. Harrison, and S. Roy, "A low-frequency versatile wireless power transfer technology for biomedical implants," *IEEE Transactions on Biomedical Circuits and Systems*, vol. 7, no. 4, pp. 526–535, 2013.

[63] A. K. RamRakhyani, S. Mirabbasi, and M. Chiao, "Design and optimization of resonance-based efficient wireless power delivery systems for biomedical implants," *IEEE Transactions on Biomedical Circuits and Systems*, vol. 5, no. 1, pp. 48–63, 2011.

[64] S. Y. Choi, B. W. Gu, S. Y. Jeong, and C. T. Rim, "Advances in wireless power transfer systems for roadway-powered electric vehicles," *IEEE Journal of Emerging and Selected Topics in Power Electronics*, vol. 3, no. 1, pp. 18–36, 2015.

[65] M. Jufer, "Electric drive system for automatic guided vehicles using contact-free energy transmission," in *2008 13th International Power Electronics and Motion Control Conference*, pp. 1–6, 2008.

[66] L. Xue, V. Galigekere, G.-j. Su, R. Zeng, M. Mohammad, E. Gurpinar, S. Chowdhury, and O. Onar, "Design and analysis of a 200 kw dynamic wireless charging system for electric vehicles," in *2022 IEEE Applied Power Electronics Conference and Exposition (APEC)*, pp. 1096–1103, 2022.

[67] W. H. Hayt, *Engineering Electromagnetics*. Mcgraw-Hill Series in Electrical Engineering. Electromagnetics, New York : McGraw-Hill, 5th ed., 1989.

[68] E. Jordan and K. Balmain, *Electromagnetic Waves And Radiating Systems 2Nd Ed.* Prentice-Hall electrical engineering series, Prentice-Hall Of India Pvt. Limited, 1995.

[69] W. H. Ko, S. P. Liang, and C. D. F. Fung, "Design of radio-frequency powered coils for implant instruments," *Medical and Biological Engineering and Computing*, vol. 15, pp. 634–640, nov 1977.

[70] T. Ono, Q.-T. Duong, Y. Kaneko, T. Higashino, and M. Okada, "Positioning using hybrid inductively-capacitively coupled parallel line feeder," *IEEJ Transactions on Electrical and Electronic Engineering*, vol. 15, pp. 304–310, 2019.

[71] "Wireless electric vehicle charging technology | halo & power transfer | qualcomm." https://www.qualcomm.com/solutions/automotive/wevc. (Accessed on 01/15/2017).

[72] U. Eberle and R. Von Helmolt, "Sustainable transportation based on electric vehicle concepts: a brief overview," *Energy & Environmental Science*, vol. 3, no. 6, pp. 689–699, 2010.

[73] A. Wiederer and R. Philip, "Policy options for electric vehicle charging infrastructure in c40 cities," 2010.

[74] T.-E. Stamati and P. Bauer, "On-road charging of electric vehicles," in *Transportation Electrification Conference and Expo (ITEC), 2013 IEEE*, pp. 1–8, June 2013.

[75] J. Boys, G. Covic, and A. Green, "Stability and control of inductively coupled power transfer systems," *IEE Proceedings - Electric Power Applications*, vol. 147, pp. 37–43, Jan 2000.

[76] J. Shin, B. Song, S. Lee, S. Shin, Y. Kim, G. Jung, and S. Jeon, "Contactless power transfer systems for on-line electric vehicle (olev)," in *Electric Vehicle Conference (IEVC), 2012 IEEE International*, pp. 1–4, March 2012.

[77] N. Stern, *The Economics of Climate Change: The Stern Review*. Cambridge University Press, 2007.

[78] F. Fattori, N. Anglani, and G. Muliere, "Combining photovoltaic energy with electric vehicles, smart charging and vehicle-to-grid," *Solar Energy*, vol. 110, pp. 438–451, 2014.

[79] S. Habib, M. Kamran, and U. Rashid, "Impact analysis of vehicle-to-grid technology and charging strategies of electric vehicles on distribution networks – a review," *Journal of Power Sources*, vol. 277, pp. 205–214, 2015.

[80] O. C. Onar, J. M. Miller, S. L. Campbell, C. Coomer, C. P. White, and L. E. Seiber, "A novel wireless power transfer for in-motion ev/phev charging," in *2013 Twenty-Eighth Annual IEEE Applied Power Electronics Conference and Exposition (APEC)*, pp. 3073–3080, March 2013.

[81] F. F. A. van der Pijl, M. Castilla, and P. Bauer, "Adaptive sliding-mode control for a multiple-user inductive power transfer system without need for communication," *IEEE Transactions on Industrial Electronics*, vol. 60, pp. 271–279, Jan 2013.

[82] F. van der Pijl, P. Bauer, and M. Castilla, "Control method for wireless inductive energy transfer systems with relatively large air gap," *IEEE Transactions on Industrial Electronics*, vol. 60, pp. 382–390, Jan 2013.

[83] A. Goldsmith, *Wireless communications*. Cambridge university press, 2005.

[84] A. Ahlbom, U. Bergqvist, J. Bernhardt, J. Cesarini, L. Court, M. Grandolfo, M. Hietanen, A. McKinlay, M. Repacholi, D. Sliney, J. Stolwijk, M. Swicord, L. Szabo, M. Taki, T. Tenforde, H. Jammet, R. Matthes, and I. C. N. R. Protectio, "Guidelines for limiting exposure to time-varying electric, magnetic, and electromagnetic fields (up to 300 GHz)," *HEALTH PHYSICS*, vol. 74, pp. 494–522, Apr 1998.

[85] Keysight Technologies, "Empro 3d em simulation software." http://www.keysight.com/en/pc-1297143/empro-3d-em-simulation-software.

[86] M. Zellagui and A. Chaghi, "Impact of series compensation insertion in double hv transmission line on the settings of distance protection," *Scientific& Engineering Research Electrical*, vol. 2, no. 8, 2011.

[87] R. Gouws, "Investigation and efficiency analysis of a 405 km transmission line with series compensation," in *2011 Proceedings of the 8th Conference on the Industrial and Commercial Use of Energy*, pp. 192–197, 2011.

[88] M. E. V. Valkenburg and W. M. Middleton, *Reference Data for Engineers Radio, Electronics, Computers and Communications.* Elsevier Science & Technology Books, 2001.

Publication List

Journal

J1. William-Fabrice Brou, Duong Quang Thang, Minoru Okada, "Efficiency analysis for inductive power transfer using segmented parallel line feeder," *IEICE Transactions on Electronics*, vol. advpub, p. 2022ECP5013, 2022.

International conferences

I1. William-Fabrice Brou, Duong Quang Thang, Minoru Okada, "Multiple-input multiple-output dynamic charging using multiple parallel line feeders," *2016 International Workshop on Antenna Technology (iWAT)*, Cocoa Beach, FL, 2016, pp. 182-185.

I2. William-Fabrice Brou, Duong Quang Thang, Minoru Okada, "Experimental evaluation of inductive power transfer system using multiple concatenated parallel-line-feeder segments," *2016 International Symposium on Antennas and Propagation (ISAP)*, Okinawa, 2016, pp. 510-511.

Domestic conferences

D1. Takuya Maekawa, Shun Iharaki, Takuya Okamoto, William-Fabrice Brou, Yuya Kaneko, Quang-Thang Duong, Takeshi Higashino, and Minoru Okada, "Demonstration of dynamic charging using double parallel line feeder," in *Proceedings of the IEICE General Conference*, vol. 2016, Mar. 2016.

D2. William-Fabrice Brou, Duong Quang Thang, Minoru Okada, "A study on inductive power transfer using multiple coupled transmission line segments," in *IEICE Technical Report on Wireless Power Transfer*, Kyoto vol. 116,no. 238, pp. 95-99, Oct. 2016.